

University of Nebraska - Lincoln

DigitalCommons@University of Nebraska - Lincoln

Mechanical (and Materials) Engineering --
Dissertations, Theses, and Student Research

Mechanical & Materials Engineering,
Department of

Summer 7-16-2021

THERMAL & MECHANICAL ANALYSIS OF BOMBYX MORI SILK NANOFIBERS

Justin Busnot

University of Nebraska - Lincoln, jbusnot2@huskers.unl.edu

Follow this and additional works at: <https://digitalcommons.unl.edu/mechendis>



Part of the [Materials Science and Engineering Commons](#), and the [Mechanical Engineering Commons](#)

Busnot, Justin, "THERMAL & MECHANICAL ANALYSIS OF BOMBYX MORI SILK NANOFIBERS" (2021).
Mechanical (and Materials) Engineering -- Dissertations, Theses, and Student Research. 171.
<https://digitalcommons.unl.edu/mechendis/171>

This Article is brought to you for free and open access by the Mechanical & Materials Engineering, Department of at DigitalCommons@University of Nebraska - Lincoln. It has been accepted for inclusion in Mechanical (and Materials) Engineering -- Dissertations, Theses, and Student Research by an authorized administrator of DigitalCommons@University of Nebraska - Lincoln.

THERMAL & MECHANICAL ANALYSIS OF BOMBYX MORI SILK
NANOFIBERS

by

Justin Busnot

A THESIS

Presented to the Faculty of
The Graduate College at the University of Nebraska
In Partial Fulfillment of Requirements
For the Degree of Master of Science

Major: Mechanical Engineering and Applied Mechanics

Under the Supervision of Professor Yuris Dzenis

Lincoln, Nebraska

July, 2021

THERMAL & MECHANICAL ANALYSIS OF BOMBYX MORI SILK NANOFIBERS

Justin Busnot, M.S.

University of Nebraska, 2021

Advisor: Yuris Dzenis

This thesis presents a study on the thermomechanical properties of Bombyx Mori silk nanofibers. These nanofibers were obtained from silkworm cocoons which were degummed to separate the fibroin and the sericin, the two proteins that make up silk. The fibroin was then centrifuged to remove insoluble particles and stored at 4°C before the electrospinning process.

A parametric study of the electrospinning process was carried out in order to identify the factors allowing to obtain optimal mechanical properties. The current as well as the flow rate applied, the diameter of the syringe, the distance separating the syringe from collector or even the environmental conditions and the concentration of the solution are all parameters influencing the specific characteristics of the nanofibers obtained, in particular their diameter, their distribution and their orientation.

A range of concentrated solutions from 1% to 6% silk fibroin were prepared with Hexafluoroisopropanol (HFIP) as a solvent. These solutions were electrospun using process

parameters which corresponded to the best conditions for electrospinning. The morphologies of these nanofibers were characterized by scanning electron microscopy (SEM). Their mechanical properties have also been evaluated using the lab nanomechanics testing system specially designed for single fiber tensile testing enabling to link the influence of electrospinning parameters to the final properties of silk nanofibers.

The thermal properties of the degummed silk fibroin were also investigated using differential scanning calorimetry (DSC) which allowed to determine the specific phase transitions and crystallinity of degummed silk fibroin and silk nanofibers. Moreover, Raman spectroscopy has been performed to characterize the molecular composition and the external structure of degummed silk and silk nanofibers.

ACKNOWLEDGEMENT

First of all, I would like to express my deep gratitude to my advisor Dr Yuris Dzenis who supervised me throughout this thesis and who shared his valuable advice with me. May he also be thanked for his kindness, his permanent availability and for the many encouragements he provided me throughout my Master's Thesis.

I would also like to thank Dr Nicolas Delpouve for his follow-up and his responsiveness from across the ocean as well as all my professors at the University of Rouen who encouraged me to continue my studies at the University of Lincoln Nebraska.

My thanks also go to Lucas Barry for his patience, kindness and availability who has helped and trained me many times during my research.

Finally, I would like to sincerely thank my family and friends for their tremendous support throughout my stay in Lincoln.

TABLE OF CONTENT

Chapter 1: Introduction	1
1. Problem Statement	1
2. Introduction to the study	3
3. Aims and Objectives	4
Chapter 2: Background.....	5
I. Spider Silk.....	5
1. The interest for spider silk.....	5
2. Mechanical Properties of spider silk	6
3. Recombinant spider silk	10
II. Bombyx Mori Silk.....	13
1. Formation and composition of B. Mori silk.....	13
a. Sericulture.....	13
b. Composition of Bombyx Mori silk.....	15
c. Structure of Bombyx Mori silk.....	16
2. Characterization of Silk.....	18
a. Mechanical Properties	18
b. Thermal Properties	21
Chapter 3: Materials & Methods.....	23
1. Materials.....	23

2.	Production of Silk solution.....	24
a.	Degumming Process	24
b.	Dialysis	25
c.	Centrifugation.....	26
d.	Production of silk fibroin films	27
3.	Electrospinning.....	28
a.	Solution Parameters	30
b.	Process Parameters	32
c.	Environmental Parameters.....	33
4.	Nanofiber Imaging	34
5.	Nanomechanical Testing	35
6.	Raman Spectroscopy	37
7.	Differential Scanning Calorimetry	38
Chapter 4: Results & Discussion.....		39
1.	Parametric Analysis of Electrospinning	39
a.	Influence of the concentration	39
b.	Influence of the applied current.....	45
c.	Influence of Flow rate.....	46
d.	Influence of the distance needle - collector	47
e.	Influence of needle diameter	48
2.	Nanomechanical Testing	49
3.	Raman Spectroscopy	56

4. Differential Scanning Calorimetry	60
Chapter 5: Conclusion	63
1. Current Conclusion	63
2. Future work	64
BIBLIOGRAPHY	65

LIST OF FIGURES

Figure 1: The silk glands and threads of <i>Araneus diadematus</i> . The glands are called by their Latin names, which are again referred when associated with the type of silk they produce [18].	6
<i>Figure 2: Typical stress strain curve for spider dragline silk reeled from a <i>Nephila edulis</i> female, based on experimental data. [22].....</i>	8
Figure 3: Comparison of stress-strain curves for several materials (figure modified from Gosline et al. [17])......	10
Figure 4: Generic curves (thick lines) and tensile performance envelopes (dashed bound areas) of spider dragline silk (orange), silkworm silks (light blue), reconstituted silks (light green), recombinant silks (blue) and selected synthetic polymers (PC, PET, PMMA red) [39].	12
Figure 5: Stages of life history of mulberry silk worm <i>Bombyx mori</i> . [41].....	14
Figure 6: <i>Bombyx mori</i> silk gland organization [43].....	15
Figure 7: Schematic presentation of the silk fibroin (SF) structure; d represents the diameter of a single silkworm thread [44]	17
Figure 8: Representative tensile stress-strain curves measured for different natural fibers [48]	18
Figure 9: Stress-strain curves of silk fibers classified into 5 types [48]	21
Figure 10: Cocoons used to produce silk nanofibers	23
Figure 11: A cocoon and its silkworm	23
Figure 12: Dialysis of the silk solution	26
Figure 13: Silk Fibroin film	27
Figure 14: Diagram of the electrospinning process [56].....	29

Figure 15: Sample preparation procedure and calibration of the nanomechanics testing system. (a) Schematic of the window collector and the procedure for obtaining individual NFs; (b) schematic of sample preparation for mechanical testing and diameter measurement; (c) NF mounted on the grips of the nanomechanics testing system; (d) calibration curve obtained by measuring the force exerted by pre-weighted steel foil samples [67].	36
Figure 16: DSC 204 F1 Phoenix	38
Figure 17: Average nanofiber diameter vs silk fibroin concentration	43
Figure 18: Diameter distribution of 2% silk fibroin nanofibers	44
Figure 19: Diameter distribution of 1% silk fibroin nanofiber	44
Figure 20: Average nanofiber diameter vs Applied current	45
Figure 21: Average nanofiber diameter vs applied flow rate	47
Figure 22: Microstructure of nanofibers obtained for a flow rate of 1mL/h	47
Figure 23 : Average nanofiber diameter vs distance needle - collector	47
Figure 24: Average nanofiber diameter vs needle diameter	48
Figure 25: True strength of silk fibroin nanofibers in function of their diameter	50
Figure 26: Toughness of silk fibroin nanofibers in function of their diameter	51
Figure 27: Young's modulus of silk fibroin nanofibers in function of their diameter	51
Figure 28: Stress strain curves of different diameter of nanofibers. Green: 905nm. Grey: 322nm. Yellow: 201nm. Orange: 186nm. Blue: 145nm	51
Figure 29: True stress strain curve of silk fibroin nanofibers	56
Figure 30: Comparison of the true stress-true strain curves of natural spider silk and spider silk gut fibers [68]	54
Figure 31: Stress-strain curves of natural fibers. Grey: hair (42,2 μm). Yellow: Cotton (12,87 μm). Blue: Degummed Silk (11,3 μm). Orange : silk fibroin (145 nm)	54
Figure 32: Raman spectra of silk (red) and fibroin (black) fibers [72]	56

Figure 33: Raman Spectra of silk nanofibers and degummed silk.....	57
Figure 34: Raman spectra of degummed silk and of different percentage of silk fibroin nanofibers	58
Figure 35: DSC curves of degummed silk and 2% silk fibroin nanofibers.....	61
Figure 36: DSC heating curves of degummed B. mori silk fiber (black) and lyophilized silk fibroin hydrogel (red).	62

LIST OF TABLES

Table 1: Average Values of Mechanical Properties of Silk Fibers and High-Performance Synthetic Fibers [27]	9
Table 2 : Mechanical parameters of synthetic and natural fibers and steel.....	19
Table 3: Average silk nanofiber diameter and microstructure obtained after electrospinning for different concentration.....	40
Table 4: Average diameter of nanofiber obtained for different current values.....	45
Table 5: Average diameter of nanofiber obtained for different applied flow rate	46
Table 6: Average diameter obtained for a specific distance needle - collector.....	47
Table 7: Average diameter obtained for different needle diameter.....	48
Table 8: Position and Assignment of Different Bands of Silk Proteins [77]	58

Chapter 1: Introduction

1. Problem Statement

Polymeric materials can be characterized in two main families according to their origin: polymers of petrochemical origin and biosourced polymers. This classification is based on the origin of the raw material. This involves, through the use of bio-sourced materials, to develop new raw materials for the manufacture of polymer materials in order to reduce dependence on petroleum; and to find new innovative properties thanks to the infinite wealth of life. This classification therefore does not take into account the properties of the material which can be developed. These are not specific to each family.

Bio-sourced materials can be separated into three categories: natural polymers (eg cellulose, silk, chitin); polymers resulting from biotechnology (eg bacterial cellulose); and synthetic polymers (Ex: poly-lactic acid). The fiber market is only part of this field of polymer materials. And it is within this market that we find natural fibers, and silk. The natural fibers can be saccharides such as cellulose in plants (cotton, sisal, flax, etc.) or chitin in arthropods, or proteins such as wool (keratin) or silk. Silk is found in many animals in the class of insects such as Lepidoptera (butterflies), Hymenoptera (bees) or other orders of insects, the class of arachnids (spiders), and other groups of animals (mollusks). Silk is more widely part of the fibrous proteins.

The attraction for this natural / biobased polymer is growing. With a remarkable combination of stress and strain at break, silk fibers are considered the "best" natural fibers that can compete with high performance synthetic fibers, with superior qualities attributed to spider silk. Silk polymers have recently become desirable for use in biomaterials owing to their

remarkable properties. Indeed, they are mechanically strong, biocompatible, biodegradable, and can be easily shaped as various tissue scaffolds.

Their unique mechanical properties are due to the highly repetitive sequences in the fibrous proteins, which lead to homogeneous beta-sheet crystals in their secondary structures. [1-3] Even if the literature considers silk as a homogeneous material both in its structure and in its mechanical properties, the great variability of the mechanical properties is established. [4]

The remarkable mechanical characteristics of silk are not their only asset. They also exhibit good thermal and chemical stability, a certain morphological flexibility, and make it possible to consider biomedical applications (biocompatibility, controlled proteolytic biodegradability) or chemical grafts (for example to immobilize growth factors)

Fibrous proteins play an essential role in mobility, structure and protection at the cellular and tissue level, up to the level of organisms. However, despite much research, the assembly mechanisms as well as the structure of such materials remain incompletely known. And yet, the mechanical performances in particular, are very interesting. They therefore have enormous potential as technical and medical applications.

2. Introduction to the study

Silk has been a material known for thousands of years. Its fibers, although mainly used in the textile sector (because silk is naturally thin, light and pleasant to wear), are increasingly studied because of their excellent mechanical properties, their biocompatibility and their biodegradability. In addition, these attractant properties can be enhanced by various chemical modifications, which thus allow the attachment of growth factors, cell adhesion domains or other molecules of interest, to silk. Associated with the technique of electrospinning, which makes it possible to produce nanofibers, the properties of silk proteins can lead to numerous applications in the biomedical field.

Electrospinning is a technique that produces polymer nanofibers (50 to 1000 nm in diameter) and allows them to be shaped [5]. The solution rich in fibroin is subjected to a strong electric field at the exit of a syringe. This field which charges the liquid jet makes it possible to obtain a fiber under the action of electrostatic repulsions. With this technique, different properties can be controlled. Indeed, by modifying the spinning parameters (voltage, flow rate, volume) or the fibroin solution parameters (viscosity and concentration), it is possible to obtain different geometries, fiber diameter, orientation and porosity.

The final properties of silk nanofibers therefore depend on the parameters of the electrospinning process. Thus, the study of these parameters is essential to optimize these properties and allow the development of new applications of silk nanofibers.

3. Aims and Objectives

This study mainly aims to assess the influence of experimental parameters on the final properties of silk nanofibers. Several studies around silk nanofibers have already been carried out in particular in Dr Dzenis Lab. This research will expand knowledge on the subject thanks to the large amount of data obtained during the characterization of these nanofibers. The main objectives of this research were:

- The extraction and purification of fibroin. The spinning of silk fibroin can only be done from a liquid solution. The silk is first extracted and purified to separate the sericin from the fibroin and then dissolved in solution.
- A Parametric analysis of the electrospinning process of silk nanofibers. Various parameters are studied where several categories are to be distinguished: process parameters (flow rate, current, syringe diameter, syringe-collector distance, etc.), solution parameters (concentration, viscosity) and environmental parameters (temperature and humidity).
- The characterization of the thermomechanical properties of nanofibers. Evaluation of mechanical properties using nanomechanical tensile tests and thermal properties using differential scanning calorimetry (DCS).

Chapter 2: Background

I. Spider Silk

1. The interest for spider silk

In the early 1970s, the research groups of Work, Gosline and Tillinghast produced a few papers describing the physical, mechanical and chemical properties of silk thus rekindling the craze for spider silk [6]. Since the mid-1980s, scientific interest has only grown over the years. Indeed, with less than five scientific publications per year between the years 1985 and 1990, there are now more than 80 articles per year on spider silk since 2004.

Thanks to its exceptional properties, we could see a strong comeback of spider silk in the next few years. Indeed, by means of an efficient artificial spinning process perfectly mimicking that of the spider, it would be possible to produce fibers from recombinant silk proteins. We can even think of obtaining new "techno-fibers" having the desired attributes made from genetically modified proteins or even from polymer-protein mixtures [7-10].

However, to artificially reproduce fibers whose mechanical properties have been optimized during 400 million years of evolution in the spider, two major obstacles mainly arise in front of us [11]. First, you have to be able to produce silk proteins on a large scale, because breeding the spider is not an option given its low silk production and cannibalistic behavior [12]. Secondly, it is imperative to elucidate all the details of the complex spinning process taking place in nature, in order to obtain an insoluble fiber from a highly concentrated protein solution which compares mechanically in every way to that of the spider.

Scientific advances in molecular biology provided the required the tools to extract, synthesize and assemble genes allowing the production of large quantities of proteins with more or less high yields, the first objective has been partly elucidated. There remains mainly the

achievement of the second objective, which many are trying to achieve by trying to better understand all the mechanics behind the process of spinning the sericogenic solution contained in the bag of the gland, which flows along the duct, until obtaining an insoluble fiber having the mechanical properties that we know.

2. Mechanical Properties of spider silk

The exceptional mechanical properties of spider silk are the main reason for the resurgence of interest from the scientific community in this fiber. Indeed, the yarn produced by spiders is a biomaterial which has an interesting combination of mechanical properties (strength, resistance, extensibility and endurance), in particular for the weft yarn [13-15]. This precision is all the more important as the spider can produce up to 7 types of silk with different mechanical properties suitable for various vocations [16-18].

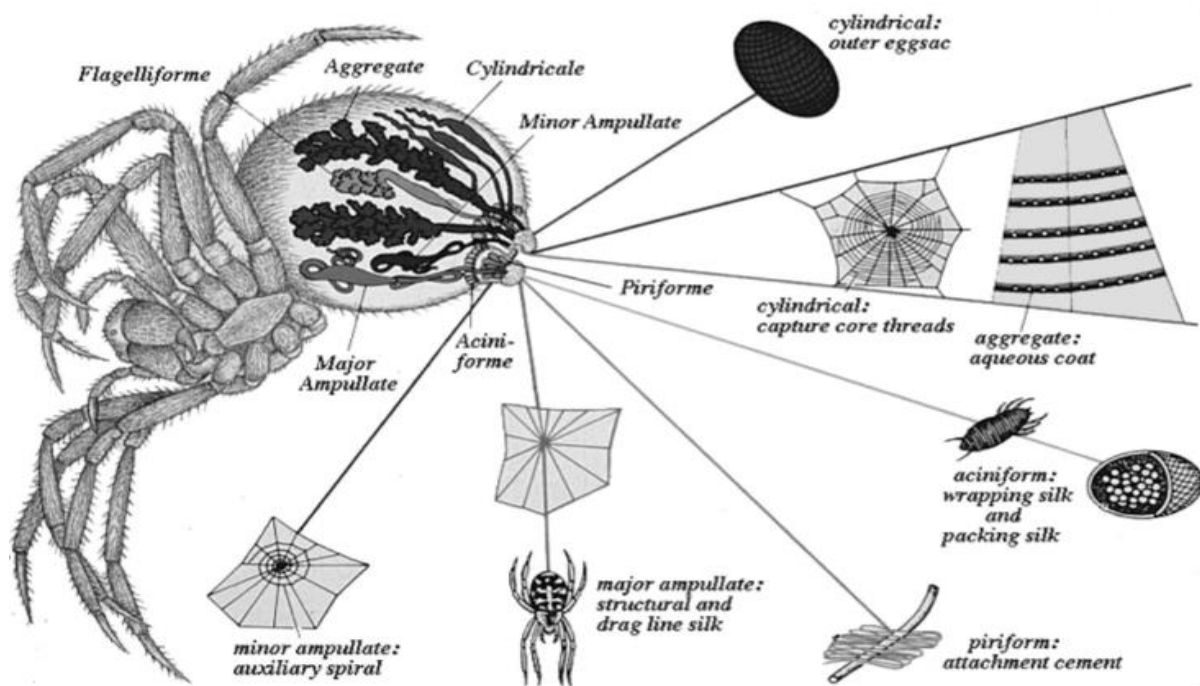


Figure 1: The silk glands and threads of *Araneus diadematus*. The glands are called by their Latin names, which are again referred when associated with the type of silk they produce [18].

Figure 1 illustrates the sericogenic glands of a spider weaving orbicular webs as well as the types of silk it produces. It can be seen that the weft thread is mainly produced for the construction of the very structure of the web (frame and spokes) as well as for the survival thread during a rapid vertical descent [19]. The aciniform glands produce the thread to wrap the prey, while the silk used to make the spider's cocoon comes from the cylindriform glands. In addition, it is the flagelliform and aggregated glands which respectively synthesize the proteins of the very extensible thread of the spirals of the web to intercept the prey in flight as well as the sticky coating to retain them [20-21].

In order to be able to compare the mechanical properties of various materials with each other, it is important to understand the meaning of the various terms used in the field. To do this, here is a brief description of the vocabulary used in the field of textiles and polymers, both natural and synthetic.

First, Figure 2 illustrates schematically a typical tensile experiment performed on a material; this is the curve of the stress as a function of the strain. The stress of a material (σ) is the force applied to this material per unit area, and it is expressed in Pascal. When a stress is applied, the sample undergoes a strain (ϵ), which corresponds to a certain percentage of its initial length $(\frac{L}{L_0} - 1) \times 100$. For low stresses, the strain is said to be elastic, i.e., the material returns to its initial state when the stress is removed and, in this linear domain, it follows Hooke's law:

$$\sigma = E \cdot \epsilon$$

where E is the slope of the elastic strain, which is also called Young's modulus or initial modulus. The term used to denote the value of Young's modulus is the strength of the material, so the higher the initial modulus, the better the strength of the material. Other terms are commonly used to designate the mechanical properties of certain fibers. The strength and

extensibility of a material are used to qualify the stress and strain at the point of failure of the material, respectively. Finally, the term toughness is used to quantify the fracture energy of a material corresponding to the area under the stress-strain curve.

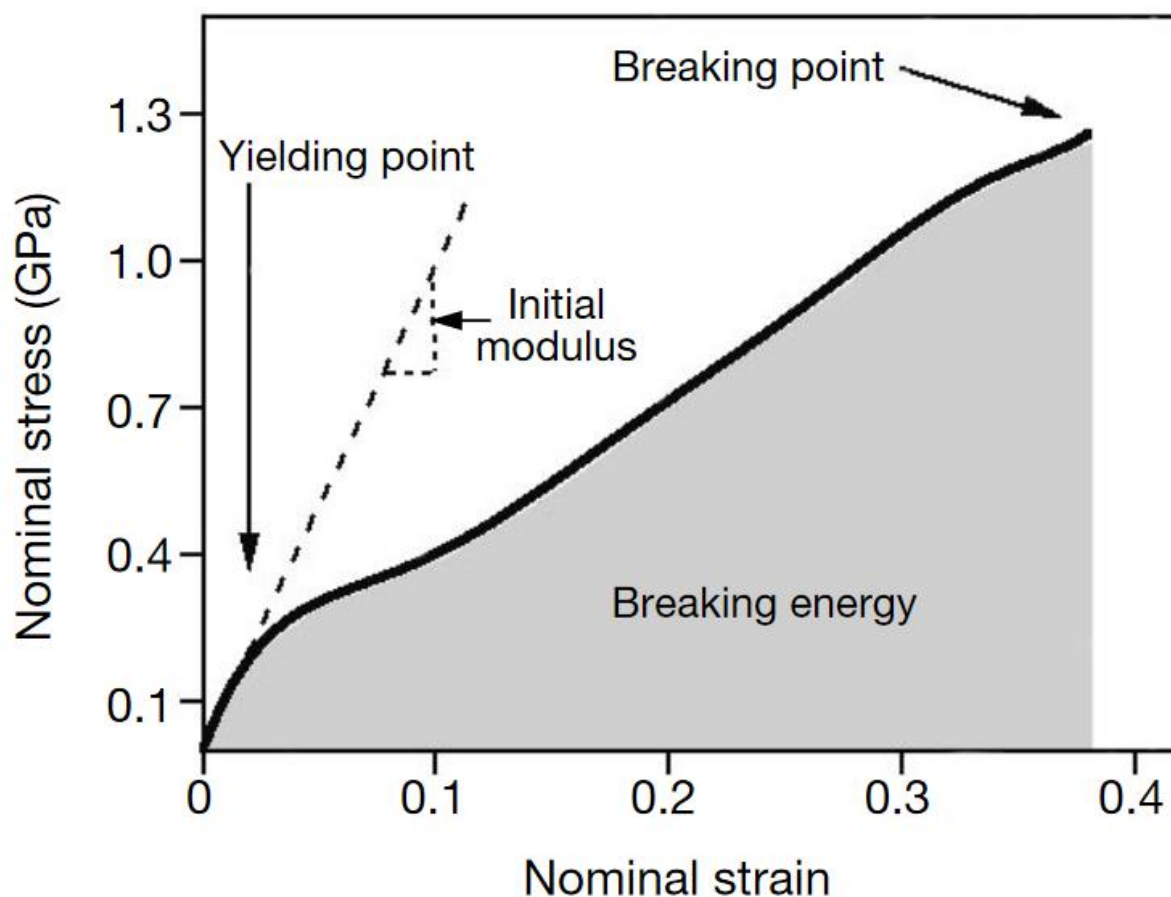


Figure 2: Typical stress strain curve for spider dragline silk reeled from a *Nephila edulis* female, based on experimental data. [22]

It is moreover this last characteristic which is particularly exceptional in the case of the weft thread of the spider, because it can thus dissipate a large quantity of energy before giving way. This property could be very interesting for several industrial applications, in particular for making bulletproof vests less heavy than those currently used, as support cable of all kinds, as well as for the production of fishing lines. Other applications are also conceivable in the biomedical field given its biocompatibility, more particularly for the production of suture as well as as a matrix for the support of cells in tissue engineering [23-25].

In order to better illustrate the exceptional character of spider silk, Figure 3 accompanied by Table 1 show schematically and experimentally, respectively, the comparison between various types of silk and synthetic fibers commonly used. In the light of the scientific data collected, it can be seen that spider silk, despite a density 6 times lower, has a tensile strength similar to that of steel. It was also observe that spider silk has an extensibility equivalent to more than ten times that of Kevlar 49®, for a total endurance of 165 MJ-m³, or three times that of Kevlar (50 MJ-m³) and 25 times that of steel (6 MJ- m³) [26-27].

It is also noted that although the silk of the Bombyx mori silkworm has a higher stretchability than many types of fiber, the combination of its stretchability and strength is much lower than that of spider silk. This incredible combination of mechanical properties is undoubtedly directly related to the optimization of several parameters, including the composition and structural organization of fiber proteins during the spinning process, still poorly understood by the scientific community [28].

Table 1: Average Values of Mechanical Properties of Silk Fibers and High-Performance Synthetic Fibers [27]

Fiber type	Density (g/cm³)	Modulus of Elasticity E (GPa)	Tensile Strength σ_R (GPa)	Breaking Strain ϵ_R (%)	Resilience (MJ/m³)
Spider silk					
Argiope trifasciata	1.3	1–10	1.2	30	100
Nephila clavipes	1.3	1–10	1.8	30	130
Silkworm silk					
Bombyx mori	1.3	5	0.6	12	50
Nylon 6.6	1.1	5	0.9	18	80
Kevlar 49	1.4	130	3.6	3	50
PBO	1.6	270	5.8	3	70
Steel	7.8	200	3.0	2	6

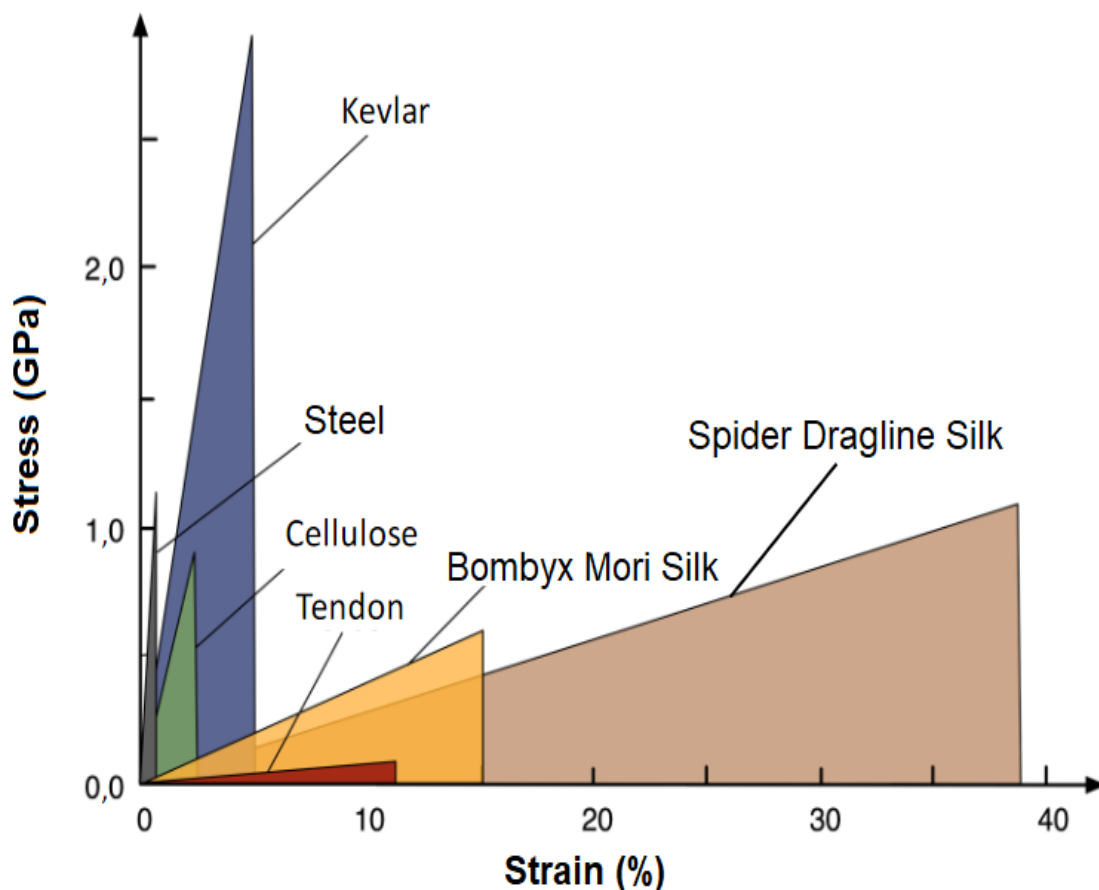


Figure 3: Comparison of stress-strain curves for several materials (figure modified from Gosline et al. [17]).

3. Recombinant spider silk

Given the exceptional mechanical properties unique to spider silk, it would be interesting to be able to produce it industrially. However, spiders are cannibals, so it is very difficult to domesticate them. In addition, the spider does not produce a very large amount of silk and it must live in an environment with controlled humidity and temperature. It would therefore be too costly for the industry to market this type of breeding. In order to find a more efficient way to produce silk in large quantities, molecular biology researchers succeeded in isolating the genes that code for the synthesis of spider silk and inserting them into a host system. The hosts used are generally the bacterium *Escherichia coli* (*E. coli*), potato and tobacco plants as well as mammals. This silk, obtained by genetic modifications, is called recombinant silk.

Several research groups have produced spider silk using the *E. coli* vector [29-32]. They chose this host system since it handles well, gene duplication is rapid, and the bacteria are readily available commercially. The principle is relatively simple; genes encoding spider silk are inserted into the genes of the bacterium *E. coli*. Since the genes encoding spider silk are part of the bacteria's genetic baggage, the bacteria's cells multiply the gene by multiplying on their own. When the bacteria synthesize its proteins, it also synthesizes spider silk proteins. With biochemical purification methods, the MaSpI and MaSpII proteins of spider silk can be isolated from other components of the *E. coli* bacteria [33].

Scheller's group chose to use a plant as a vector to produce spider silk proteins. They first inserted the two genes (MaSpI and MaSpII) into the cells of tobacco and potato leaves. When the cells multiply while the leaf is growing, using messenger RNA, the genetically modified plant can synthesize both spider silk proteins. When the plant is big enough, the leaves are harvested and the spider silk protein extracted. The production of spider silk proteins through plant leaves is 10-50% greater than overexpression in *E. coli* bacteria [34-35].

The company Nexia Biolechnologies Inc. of Montreal (Nexia) has instead opted for the insertion of the genes encoding the MaSpI and MaSpII proteins in the mammary cells of a goat. The company's molecular biologists inserted the DNA sequences of these proteins into dominant genes in goat mammary cells. Being on dominant genes, spider silk proteins can be passed down from generation to generation. When the goat is in the lactation period, it expresses the MaSpI and MaSpII proteins in its milk. The recombinant proteins could be isolated from the other components of milk by precipitation and column chromatography.

This company has also succeeded in manufacturing synthetic silk fibers by wet spinning [36]. The extrusion was carried out from aqueous solutions or in organic solvents. By exerting pressure on the piston of the extruder, a thread of the protein comes out of the extruder and upon contact with methanol, the proteins coagulate and form a silk thread. With the help of a

pulley system, tension is exerted, which allows better control of the orientation of the crystalline domains in the regenerated fiber.

Recombinant proteins are found in different forms such as powder, gel, fiber and membrane. The fields of application can be just as varied: medical (suture thread, biomaterial), nanofibers, high performance textiles, food additives, cosmetics, culture medium [37-38].

However, although recombinant spider silk can be obtained through several processes, their final mechanical properties are not similar to natural spider silk. Indeed, their mechanical properties are significantly lower as shown in Figure 4. Different results can be found for the mechanical properties of silk (i.e., Figure 3 and Figure 4) but it is admitted that natural spider silk has higher mechanical properties as Bombyx Mori silk.

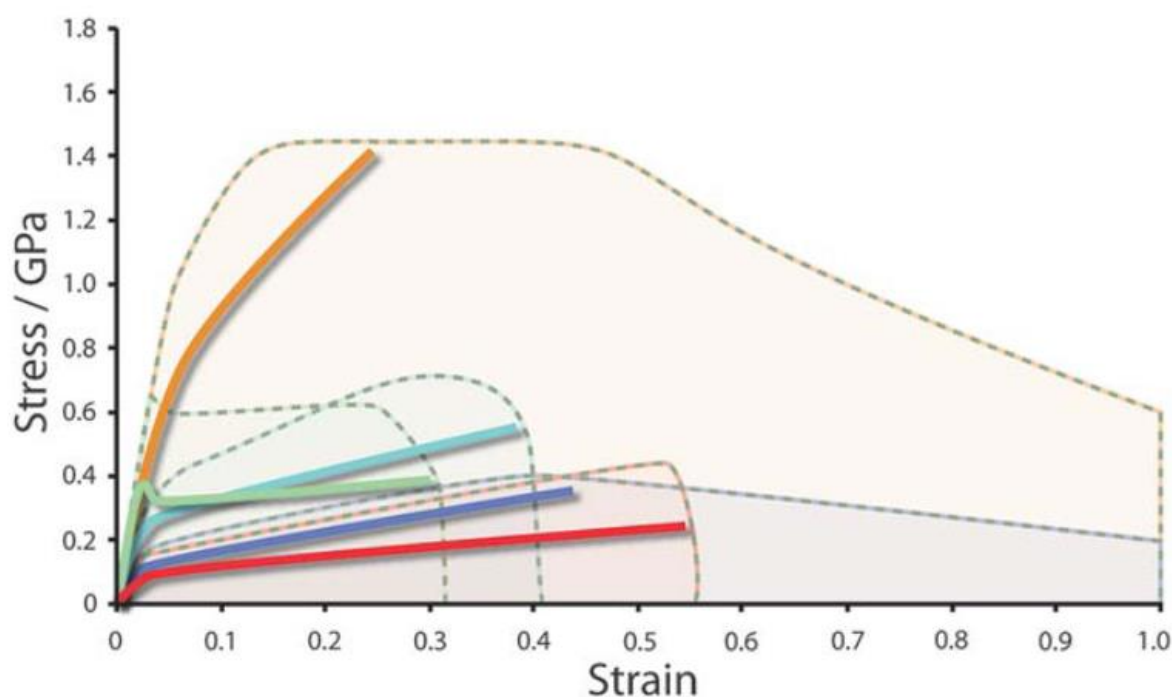


Figure 4: Generic curves (thick lines) and tensile performance envelopes (dashed bound areas) of spider dragline silk (orange), silkworm silks (light blue), reconstituted silks (light green), recombinant silks (blue) and selected synthetic polymers (PC, PET, PMMA red) [39].

Faced with such a finding, other alternatives to recombinant spider silk have been considered to approach the exceptional properties of natural spider silk. Research has therefore turned to reducing the diameter of natural silk and mainly Bombyx Mori silk, which is much easier to

produce in large quantities. The main motivation for this research lies in the fact that a reduction in the diameter of the fibers leads on the one hand to smaller fiber defects but also to a lower probability of having defects and therefore to a better resistance of the fibers to mechanical stresses. Thus, this report deals with the production and evaluation of the properties of Bombyx Mori silk fibroin nanofibers.

II. Bombyx Mori Silk

1. Formation and composition of B. Mori silk.

a. Sericulture

The original silkworm species used is the wild silkworm *Bombyx mandarina* which domestically gave rise to *Bombyx mori*. While current yields reach cocoons producing over 1600m of yarn, the cocoons originally were expected to produce between 100 and 150m. It was through extensive selection that man was able to domesticate the silkworm, obtaining a poorly mobile worm, and a butterfly incapable of flight and therefore of reproducing without human help.

The development cycle of *Bombyx mori* is broken down into several phases: the egg; larval stages; the pupal stage; and the adult. These four phases are separated by molts and metamorphosis of the chrysalis to give the butterfly. The larval phases last about twenty days and are made up of 5 stages separated by molts. These molts allow an increase in the volume of the worm and the continuity of growth. The metamorphosis lasts about ten days and allows a reorganization of the chrysalis in the cocoon to form the butterfly. In the adult stage, individuals seek to reproduce in order to lay eggs and allow a new cycle (Fig.5).[40]

For the production of cocoons, the worms are placed on racks which are covered with mulberry leaves. Indeed, the worms of *Bombyx mori* feed exclusively on this type of

vegetation. They can thus grow optimally. When they reach the fifth stage, they are moved to appropriate devices to facilitate the production of their cocoon. The cocoons are then harvested by the sericulturist who delivers them to the spinning mill. Upon receipt, after control, the cocoons are steamed to kill the chrysalis and prevent it from turning into a butterfly. Indeed, to get out, the latter would pierce the cocoon and cut the continuous thread of which it is made. The cocoons can then be stored.

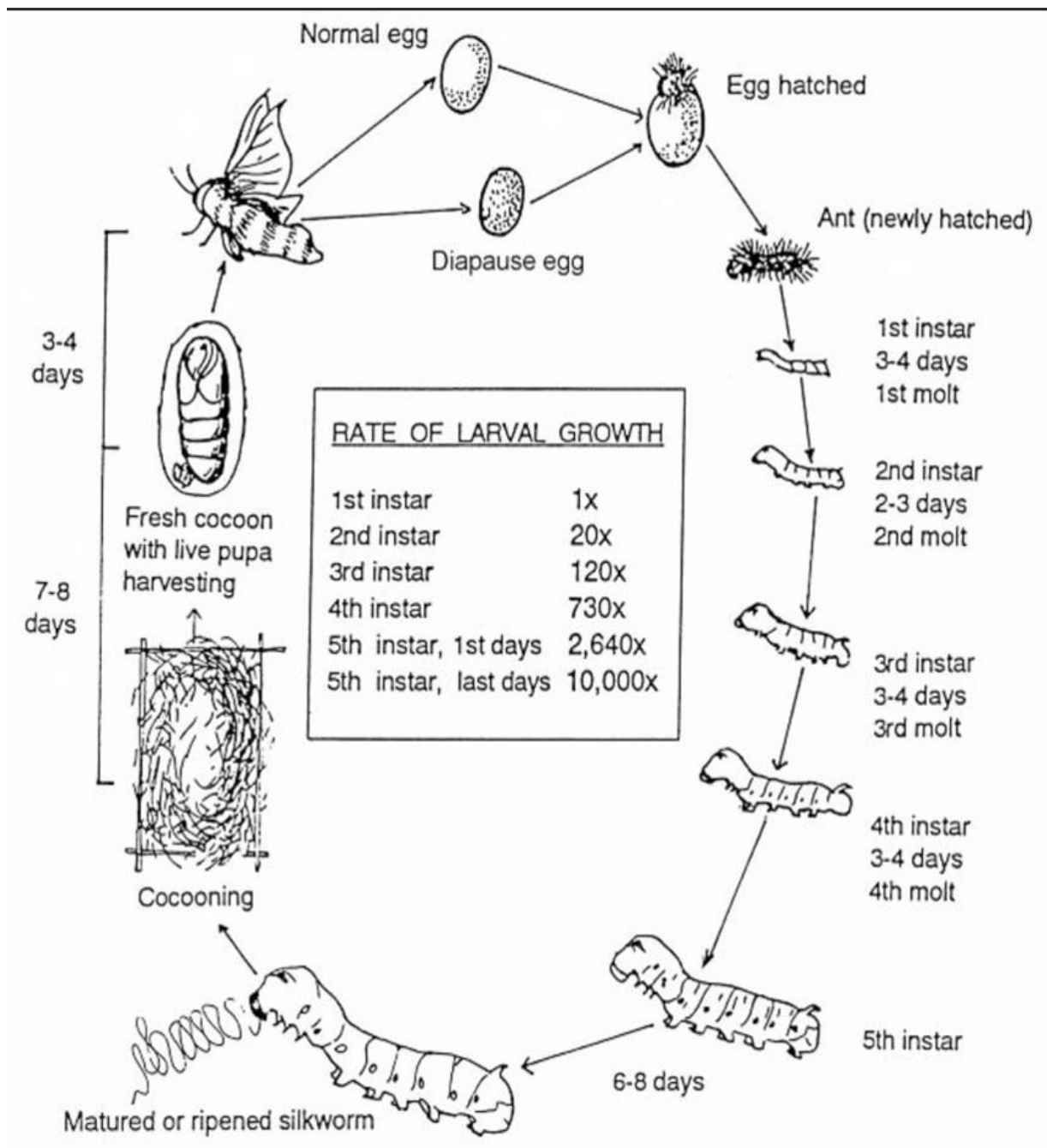


Figure 5: Stages of life history of mulberry silk worm *Bombyx mori*.[\[41\]](#)

b. Composition of Bombyx Mori silk

Silk is a thread made up of two strands wrapped in a sheath. The whole system is made up of proteins. At first glance, it can be considered that the strands are made of fibroin and that the sheath, also called sandstone, is made up of sericin. The production of silk thread by the worm consists of protein synthesis followed by storage; then spinning the gel to form the thread and make the cocoon. Silk, which is protein in nature, is synthesized by two so-called silk glands, symmetrical, open to the outside by the sector.

These silk glands can be divided into three distinct parts: posterior, middle and anterior (Fig.6). They are made up of exocrine cells that can synthesize and then secrete the product of their synthesis into the lumen outside the cell. The posterior part synthesizes fibroin. The middle part which can itself be subdivided into three sections produces three types of sericins which will envelop the fibroin previously produced.

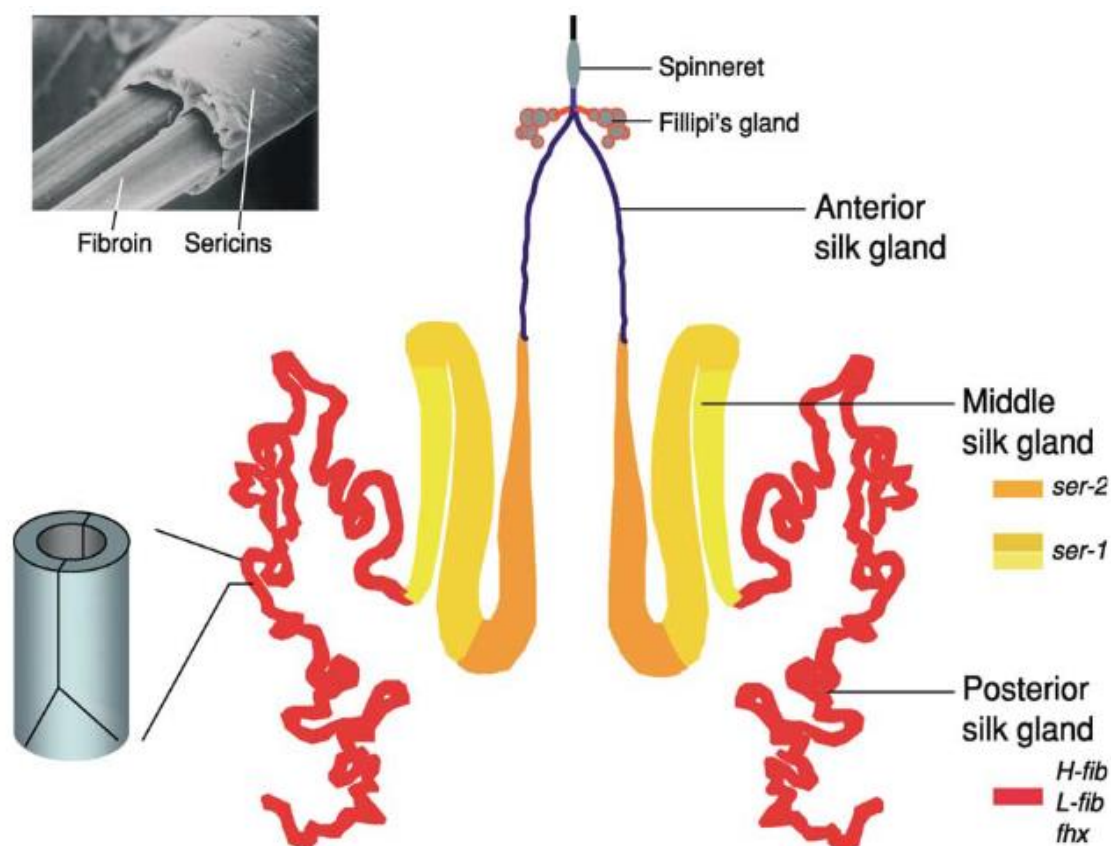


Figure 6: Bombyx mori silk gland organization [43]

The silk is therefore presented as a coaxial, the central part of which is composed of fibroin and the external part of sericin. The last part, anterior, does not produce any protein, it is covered with a thin cuticle (protective wall). It is only a conduit leading to the final part formed by the spinneret [42].

c. Structure of Bombyx Mori silk

As stated above, silk is essentially made up of two proteins: fibroin and sericin. Fibroin forms the central part of the strand while sericin surrounds the central part. However, sericin is not the source of the mechanical properties of silk. Its main role is being the gum covering the fibers and allowing them to stick together. The main properties of silk are based on fibroin.

Fibroin is a fibrous protein whose composition and structure give silk thread its qualities. It is a set of polypeptide chains organized in folded antiparallel β sheets. The primary structure of this protein is defined by a succession of the glycine - alanine - glycine - alanine - glycine - serine (GAGAGS)_n repeating units. This highly crystalline structure essentially contains hydrogen bonds that organize amino acids (AA) in the form of helices. The repeating sequence of amino acids results in a strongly coherent structure that gives silk thread its unique properties. There are two regions that exhibit repeating amino acid sequences: an alanine-rich sequence and a glycine-rich sequence.

The form of a folded structure called the beta sheet taken by the protein is due to the sequence rich in alanine. It looks like an accordion sheet of paper. When the silk protein folds back, the beta sheets juxtapose to produce a fibrous protein which confers some of the interesting mechanical properties of silk. This type of crystal structure is called type II silk. It is an antiparallel beta sheet structure, belonging to the monoclinic system [44].

The second existing conformation is in the form of type II β -turns, also called type I silk. It constitutes the remainder of the precipitated fraction and is found in the soluble fraction. It is also present from the start, during storage in the glands and results in the formation of type II silk. It is a metastable structure with spatial conformation with a crank or zigzag S structure, belonging to the orthorhombic system (Fig. 7) [45].

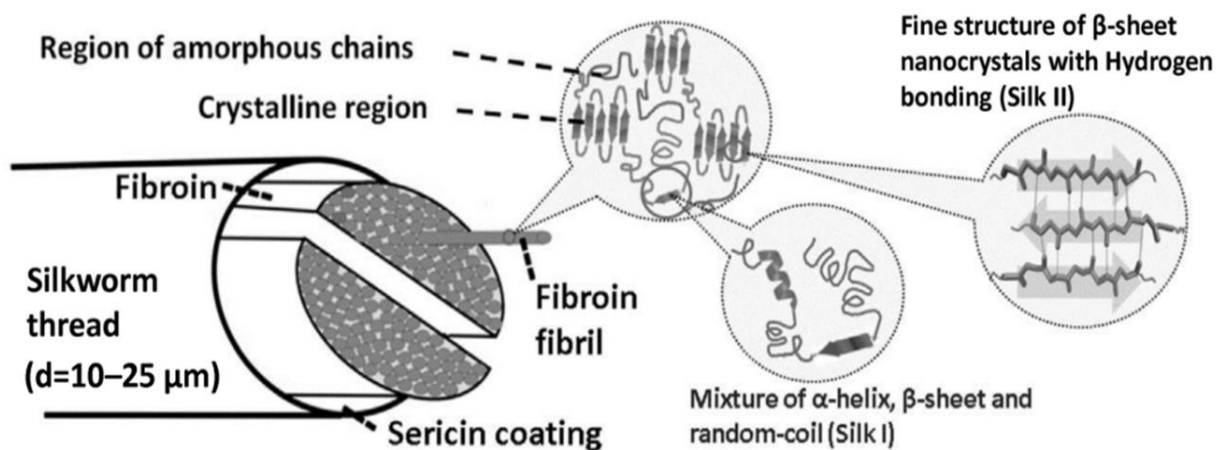


Figure 7: Schematic presentation of the silk fibroin (SF) structure; d represents the diameter of a single silkworm thread [44]

Finally, the rest of the structure is composed of α -helices and amorphous in structure. Finally, a very particular conformation has been observed under certain conditions, in particular the interfaces, called type III. But its study is limited to the understanding of experimental anomalies but does not shed any light on the understanding of microstructural phenomena.

At the level of the worm, everything is therefore in place to control the material produced and its microstructure. First, by keeping the fibroin liquid during the production and storage phase. Then by causing the conformational transition to induce the final microstructure and mechanical properties of the wire produced [46].

2. Characterization of Silk

a. Mechanical Properties

The uni-axial tensile test is the most common test used to characterize the mechanical behavior of a fiber. Indeed, measuring the compression is much more difficult. The test consists in subjecting a test piece to an elongation (ΔL) by the relative displacement of its ends and in measuring the force (F) necessary for this elongation. [47]

Figure 8 illustrates an example of a stress-strain curve obtained by this type of test. The stress (σ) is defined by $\sigma = F / S_0$, where F denotes the exerted force and S_0 the area of a cross section of the fiber. The strain (ϵ) is the relative elongation, defined by $\epsilon = \Delta L / L_0$, where L_0 is the initial length and ΔL is the length variation following stretching.

The initial slope of the stress-strain curve informs about the stiffness / flexibility of the material (Young's modulus, E). The stress (σ^{\max}) and strain (ϵ^{\max}) at break are the maximum values of stress and strain at the point where the material breaks. The area under the stress-strain curve represents the energy required to break the material.

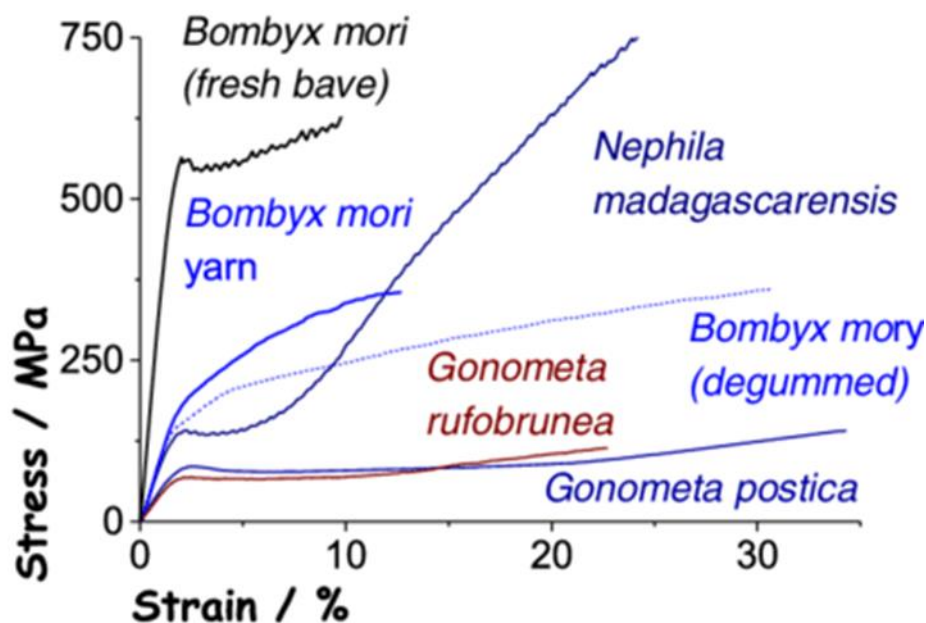


Figure 8: Representative tensile stress-strain curves measured for different natural fibers [48]

Table 2 compares the mechanical characteristics of different natural and synthetic polymeric fibers with those of steel and some ceramic fibers. There is great variability for natural fibers. This variability concerns not only the stress and the strain at break, very dependent on the pre-existing defects, but also on the shape of the curve and the value of the slope at the origin (the initial Young's modulus), intrinsic quantities of the material. studied while the first quantities are object characteristics.

Silks have a lower breaking stress than several synthetic materials (carbon fibers, Kevlar, steel) but their extensibility guarantees them a strong breaking work.

Table 2 : Mechanical parameters of synthetic and natural fibers and steel

Sample		Diameter (μm)	Young's Modulus (GPa)	Ultimate Stress (MPa)	Ultimate Strain (%)	Impact Energy (MJ/m ³)	References
Synthetic Fibers	Polyamide 66	20	5	1000	20	80	a, b
	Polyester (PET)	15	15	800	15	N/A	a
	Kevlar 49	12	135	3000	2,5	50	a, i, j
	Carbon	5	300	500	1,3	25	j
	Nicalon (Si-C-O)	14	220	3000	N/A	N/A	p
	3M Nextel 610 (Al ₂ O ₃)	10 - 12	380	3100	N/A	N/A	p
	Glass	30	68,9	3310	4,8	N/A	q
Natural Fibers	Cotton	10 - 27	8	600	7	N/A	a
	Wool	15 - 40	2	170	35	N/A	a
	Hair	80	6,6	230	40	N/A	l
	Collagen (tendons)	N/A	1,2	120	13	6	i
	Bombyx mori Fibroïn	10 - 15	5-57	320 - 1410	4 - 35	70	b, k, m, n, o
	Spidroïn	3 - 8	11 - 13	800 - 1500	15 - 39	96 - 230	b, c, d, e, f, g, h, k
Metal	High Strength Steel	-	200	1500	0,8	6	i, j

References: a) [Bunsell 2009]; b) [Gosline et al. 1999]; c) [Sirichaisit et al. 2003]; d) [Vollrath et al. 2001]; e) [Madsen et al. 1999]; f) [Lawrence et al. 2004]; g) [Madsen et Vollrath 2000]; h) [Swanson et al. 2006]; i) [Gosline et al. 2002]; j) [Gordon 1988]; k) [Pérez-Rigueiro et al. 2000]; l) [Paquin et Colomban 2007]; m) [Zhao et al. 2007]; n) [Kawahara et al. 1996]; o) [Asrar et Hill 2002]; p) [Schawaller et al. 2012]; q) [Sathishkumar et al. 2014].

Different behaviors are in fact observed for the same species, which can be classified into five types, of which Figure 9 shows the signatures:

- Type I consists of an elastic behavior up to ~ 2 to 4% for both bristles and keratins, then a plateau until breakage. This type is dominant for very fresh silk fibers, in particular manually extracted.
- Type II consists of two elastic behaviors, the first of higher modulus up to about 1.5% and the second up to about 6% and then a quasi-plateau until failure. This type is observed for slime (non-eliminated sericin sheath) and also for fibers which have been involuntarily put in tension during handling.
- Type III has a high strain, a lower initial Young's modulus and a stress at break with a gradual transition of the elastic regime (<2%) to a quasi-plateau. This signature is characteristic of wet fibers.
- Type IV shows an elastic regime below 2 to 4%, followed by a plateau and then an increase in Young's modulus (analogous to the structural hardening of metals) until failure. This behavior is observed for the wet and then dried fibers. The curve of a semi-crystalline synthetic polyamide like PA66 or PET is type IV.
- Type V shows a break in the elastic part and is observed for very degraded fibers due to heat treatment or aggressive dyeing [49].

Hair and wool, natural protein fibers based on keratin, mainly exhibit type III (water saturation) or IV behavior.

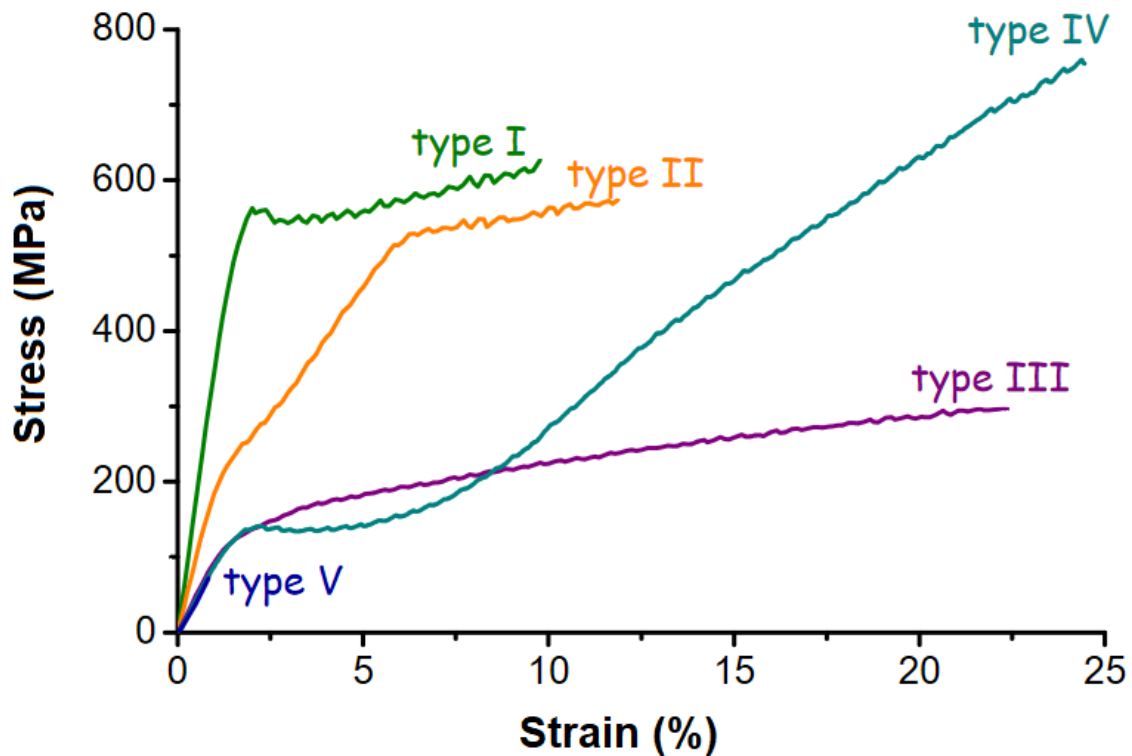


Figure 9: Stress-strain curves of silk fibers classified into 5 types [48]

b. Thermal Properties

A great deal of information can also be provided by temperature tests. Indeed, Differential scanning calorimetry (DSC) is an in-situ characterization technique that measures the heat flux that occurs during the change of state accompanied by an exchange of energy (heat absorbed or released) over a given time. Heat exchange measurements are tricky because it is difficult to isolate a system. Differential measurement overcomes this problem since it is differentiated by a witness placed under the same conditions and therefore undergo the same environmental disturbances. This generates a clear amplification of the detected signal.

Thus, by calorimetry (Differential Scanning Calorimetry and Temperature-Modulated Differential Scanning Calorimetry), it was possible to observe a glass transition temperature (T_g) of 178-179°C in the dry state for the amorphous phase, an exothermic peak at 212°C crystallization, and an endothermic melting-degradation peak centered at 263-264°C [50-51].

It can therefore be noted that silk is an extremely stable protein polymer. Cellular proteins are rarely stable above 50-60°C, leading to a phenomenon of denaturation, loss of spatial conformation. It is also possible to notice that there is no endothermic peak of clean crystalline fusion, because this one is certainly concomitant with the peak of degradation. The degradation is confirmed by gravimetric temperature tests, it begins approximately from 200°C.

The glass transition temperature varies according to the humidity rate and the crystallinity rate [52]. It therefore decreases by the presence of water (plasticizing effect of water) and increases by the level of crystallinity. These results shed light on the micro-structural aspect of silk with a macromolecular network connecting the crystallites to the amorphous zones.

Unlike synthetic fibers where the amorphous phase and the crystalline phase are relatively well differentiated. The two regions are linked in the fibroin leading to a two-phase material where the disordered macromolecules can come to stabilize around the existing crystallites but remain connected to the rest of the amorphous phase. This induces a limitation in the degrees of freedom of the amorphous phase justifying the impact of crystallinity on the T_g. In addition, the water seems to bind intimately to the material leading to a variation of the T_g as a function of the rate of humidity. [53].

Chapter 3: Materials & Methods

1. Materials

Silk fibroin nanofibers are originally obtained from a raw material being *Bombyx Mori* cocoons. These cocoons were purchased from the Mulberry Farms Fallbrook, CA (Fig. 10). The worms were previously killed after being steamed to prevent them from turning into butterflies (Fig. 11).



Figure 11: Cocoons used to produce silk nanofibers



Figure 10: A cocoon and its silkworm

2. Production of Silk solution

a. Degumming Process

The degumming of silk is the first and essential step in obtaining the fibroin solution. It makes possible to separate the two proteins constituting the silk cocoon: fibroin and sericin. Sericin mainly acts as a glue and keeps the fibers together. The silkworm cocoon can therefore be considered as a composite material with fibroin as reinforcement and sericin as matrix.

The degumming process first starts by bringing 2L of distilled water (dH_2O) to a boil in a glass beaker. 5g of Bombyx Mori silkworm are cut into thirds and extensively contaminated cocoons (excessive insect particulates coating the inner cocoon surface) are disposed of.

4,24g of sodium carbonate (Na_2CO_3) are measured and slowly added to the boiling distilled water volume to prevent the boiling over of water. When the sodium carbonate is completely dissolved, cocoon pieces are added to the boiling distilled water and stirred for 40 minutes using a Teflon stir bar during the boiling process

After boiling, the distilled water is carefully drained into a sink and the silk extract is wrung out by hand to remove the excess water. The silk extract is then washed 3 times for 20 minutes, each in 1L of distilled water in a lab beaker while the Teflon stir bar is used to circulate the volume within the beaker.

After washing, the silk extract is wrung out again by hand and placed under a chemical hood to allow for drying for a 12 hours period. The next day, the dried silk extract is weighed (average mass ~3,5g).

b. Dialysis

Silk fibroin fibers, extracted from *Bombyx mori* cocoons, are insoluble in water and most organic solvents. Fibroin dissolves in concentrated acidic solutions and in concentrated solutions of aqueous, organic and aqueous-organic salts. These solutions contain highly concentrated salts which must be removed by dialysis in order to prepare silk fibroin materials [54]. Hence, the dialysis is required for the production of silk nanofibers.

Accordingly, 9,3 moles of a Lithium Bromide (LiBr) solution are prepared in order to obtain a 20% weight per volume solution of silk. The necessary weight and volumes are calculated using the following equations:

- i. Silk extract weight ($\sim 3,5\text{g}$) $\times 4 = 14$ mL of total 9,3 M of LiBr Solution
- ii. $(807,705 \times 14 \text{ (LiBr volume)})/1000 = 11,31\text{g}$ of LiBr to add to the distilled water

The measured weight of Lithium Bromide is added into a beaker filled with the following volume of distilled water:

- $0,8 \times 14$ (calculated volume in i.) = 11,2 mL of distilled water

The solution is then poured into an appropriately sized graduated cylinder and the solution is brought to its final volume. The silk extract is placed into a beaker and the LiBr solution is poured over it. In this step, silk fibers need to be completely immersed and dissolved before continuing the process.

The solution is placed into a 60°C oven for 4 hours before reaching the dialysis step where 12mL of the solution are drawn up using an appropriately sized syringe. A 18G needle (inner diameter = 0,838 mm) is then placed at the end of the syringe and the solution is injected into a dialysis cassette (3500 MW cutoff, Slide-A-Lyzer, Thermo Scientific). After the cassette is filled, the remaining air is drawn out of the cassette with the emptied syringe.

The cassette is then immersed in a beaker containing 1L of distilled water (Fig. 12). The distilled water volume is changed after 1 hour, 4 hours, 8 hours and then every 12 hours three times for a total of six changes.

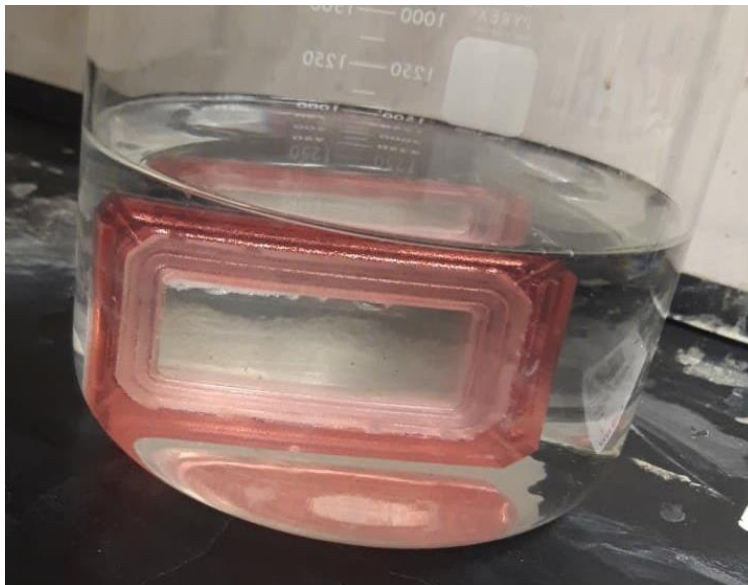


Figure 12: Dialysis of the silk solution

c. Centrifugation

After the dialysis, the silk solution is slowly collected from the cassette using a syringe. The solution is immediately placed in a 10 000g rated centrifuge tube. The solution is then centrifuged twice at 10 000g at 4°C for 20 minutes each. After each centrifugation, the supernatant is placed into a new tube. This step is done to purify the solution and getting rid of the impurities. Finally, the silk solution is stored in a 4°C refrigerator until the production of silk fibroin-based materials.

d. Production of silk fibroin films

Samples of 0,5mL of the silk solution are pipetted into a small weight dish. The weight dish is placed inside a 60°C dry oven for 12 hours, until the solution dries and films are obtained (Fig. 13). The remaining solid silk films are weighted and final silk fibroin solutions are ready to be prepared. Films are placed in a flask before being dissolved by a volume of Hexafluoroisopropanol (HFIP). The HFIP is used as a solvent for silk fibroin because of its strong polarity and its strong capacity to produce hydrogen bonds. Indeed, it is used to dissolve compounds capable of accepting these hydrogen bonds. The exact volume of HFIP is dependent on the percentage of silk fibroin of the solution.



Figure 13: Silk Fibroin film

For a specific mass concentration C of silk fibroin in the solution, the mass x of silk fibroin films thus corresponds to C of the total mass of the solution (e.g., if the wanted solution contains 6% of silk, the mass of films is equivalent to 6% of the total mass of the solution). Therefore, the mass of HFIP in the solution can be calculated with the following cross-product equation:

$$m = \frac{(1 - C) * x}{C}$$

The prepared solution is then stirred using a Teflon stir bar until the silk films are completely dissolved. Solutions also need to be electrospun in without much delay to avoid the gelation of the silk fibroin. Gelation is characterized by a sudden increase in turbidity and shear moduli of the solution. The shear modulus and turbidity of the gels increased with increasing protein concentration so higher silk fibroin solution concentration tend to transition from liquid to gel more easily. Environmental conditions also seem to influence the gelation as well as the pH of the solution. [55]

Once the silk fibroin films are completely dissolved in the HFIP, the solution is ready to be electrospun.

3. Electrospinning

Electrospinning is a nonwoven manufacturing method with many advantages for biomedical applications. This process makes it possible in particular to form nanofibers of variable sizes and orientations. Electrospinning is a process that uses electrostatic forces to make nanofibers. The elements required for its instrumentation are as follows and are shown diagrammatically in Figure 14:

- A syringe with a metal needle containing a polymeric solution or a molten polymer
- A pump to apply a defined flow rate to the solution or to the molten polymer
- A high voltage generator
- A collector connected to the earth

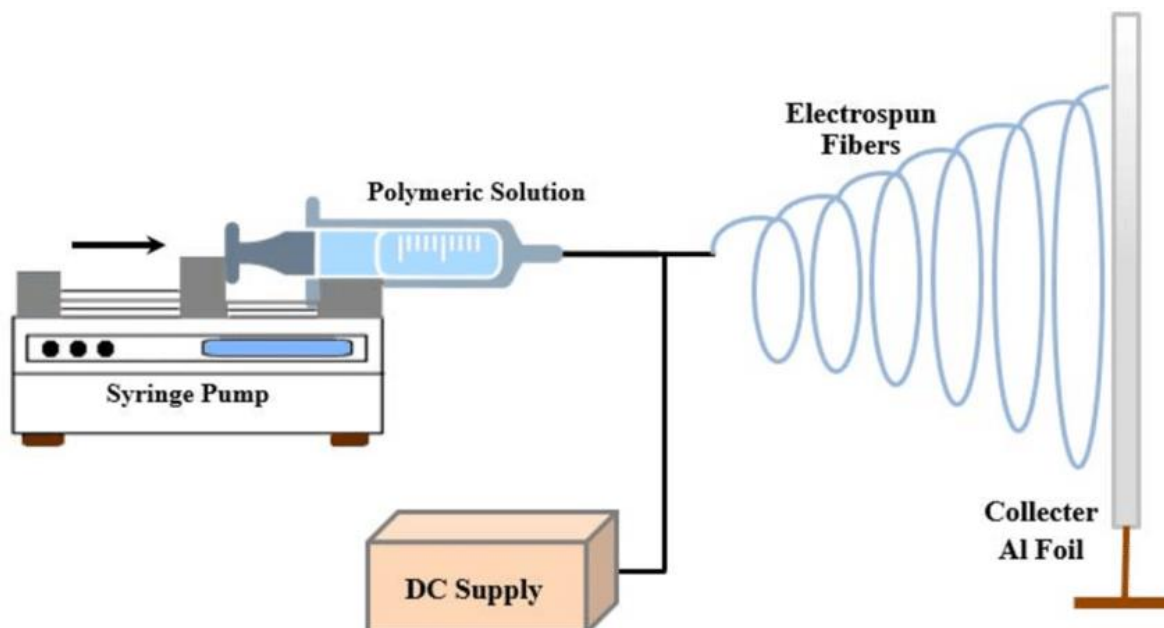


Figure 14: Diagram of the electrospinning process [56]

During electrospinning, the pump beads a drop of polymer at the tip of the needle, which is held by surface tension. The application of an electric field between the tip of the needle and the collector, using the high voltage source, induces charges in the polymer, resulting in repulsive interactions within the solution. This electrostatic force is then opposed to the surface tension of the solution. When the charge repulsion overcomes the surface tension of the solution, a jet is then projected in the direction of the collector. During the flight of this jet, the solvent in the solution evaporates and the collector then captures the resulting polymeric fibers [57].

The morphology and the diameter of the electrospun fibers depend on the various parameters inherent in the solution to be electrospun: surface tension, conductivity and viscosity. These different physical quantities depend on the molar mass of the polymer as well as on the polymer concentration of the solution to be electrospun.

The morphology and diameter of fibers also depend on process parameters such as the intensity of the applied electric field, which can be controlled by the applied current, the

distance between the needle and the collector substrate. The temperature and humidity of the atmosphere in which the experiment is conducted also control the morphology of the fibers.

In summary, the electrospinning parameters are numerous and all impact the diameter, the morphology, the distribution as well as the orientation of the nanofibers.

These parameters can be divided into three distinct categories:

- The parameters of the solution including viscosity, surface tension or conductivity
- The process parameters including the voltage and the flow rate applied but also the distance separating the needle from the collector and the diameter of the needle itself.
- The environmental parameters including the temperature as well as the humidity of the room where the electrospinning is carried out [58].

a. Solution Parameters

The viscosity of the polymer solution plays an important role in the electrospinning process. It is the critical key in determining the diameter and morphology of fibers. In general, the viscosity of the solution can be adjusted and controlled directly by adjusting the molecular weight and / or the concentration of the solution. The relationship between viscosity, concentration and molar mass is showed in the following equation:

$$C^* \sim \frac{1}{[\eta]} = \frac{1}{KM^a}$$

Where C^* is the critical concentration of the solution (concentration for which the solution is electrospinnable), $[\eta]$ is the intrinsic viscosity, M is the average viscosimetric molar mass and K and a are constants which depend on the polymer, the solvent and of the temperature [59].

Furthermore, if the viscosity is too high, the jet will break down into droplets and it will not be possible to form fibers, because the electrical charges will not be high enough to allow the fiber to be stretched [60].

Like the concentration, the molar mass of the polymer also has an important effect on the viscosity of the solution and the morphology of the fibers. At fixed concentrations, lowering the polymer molar mass tends to form beads rather than smooth fibers. Conversely, the increase in molar mass gives, after electrospinning, geometrically smooth fibers, but of micrometric diameter [61].

The conductivity of the solution is primarily determined by the type of polymer and solvent used. When choosing the solvent to dissolve the polymer, it is essential that this solvent has a certain degree of electrical conductivity. The solutions with high conductivity have a high surface charge density and are therefore more easily electrospinnable: in fact, under a given electric field, there results an increase in the elongation force on the jet which is caused by the auto repelling excess charges from the surface [62].

Surface tension is an important factor which influences the morphology of electrospun products. In fact, the surface tension controls the possibility of obtaining fibers or pearls. The higher the surface tension, the higher the probability of obtaining pearls. The surface tension depends on the nature of the solvent used.

b. Process Parameters

The formation of the jet depends primarily on the strength of the electric field applied to the tip of the needle, while the formation of fibers from the jet stream also depends on the flow of fluid and the rate of evaporation of the solvent.

Several factors inherent in the collector affect the geometry of the fibers as well as the membranes. The collector has a significant effect on the productivity, structure and arrangement of the electrospun nanofibers. The effect of the collector is based on its ability to route the charges of the deposited fibers towards the mass to discharge. With a less conductive collector, the deposited fibers can retain some of their charges which generates repulsion between the fibers resulting in reduced deposition and productivity.

The study of the effect of different support materials (polypropylene, polyethylene, polyethylene terephthalate, aluminum, acetate fibers, paper) and different shapes (flat plate, cylindrical tubes, liquid bath, gridded collector) demonstrated that the type of collector has an important influence on the number of fibers collected. The conductive collector collects more fibers, and this is probably due to the large potential difference generated between the surface of the solution and the surface of the grounded collector [63].

To form aligned fibers, the easiest method to use is to collect the fibers on a high-speed rotating cylindrical collector. The advantage of this method is to collect fibers aligned over a large area.

Another process parameter which deeply influence the electrospinning is the electric field. Indeed, the electric field is the primary factor in the electrospinning process because it affects the amount of charge applied to the solution. There are several conflicting reports on the effect of applied stress on fiber morphology and in particular on the diameter of electrospun fibers. Some studies have shown that as the voltage increases during electrospinning, the

syringe ejects more polymer solutions, which in turn increases the diameter of the electrospun fibers [64].

Other research has shown that increasing tension increases the intensity of the pull on the solution jet, which in turn promotes the formation of thinner fibers. Likewise, electrospinning with a low viscosity solution and at a higher tension can also promote the formation of secondary jets and this will also result in a smaller diameter of the fiber [65].

c. Environmental Parameters

The electrospinning environmental parameters such as humidity and temperature can also affect fiber diameters and morphology. To assess the effect of temperature on the electrospinning process, a study was carried out by heating the solutions as well as the electrospinning enclosure to temperatures varying between 30 and 60 ° C. Under these conditions and with the increase in temperature, it was found that some physical properties of the solution such as viscosity, surface tension and conductivity varied and showed different values from those at room temperature. The change in these properties affects the electrospun fibers, which leads to a decrease in the diameter of the electrospun fibers [66].

On the other hand, the effects of humidity are strongly coupled with other parameters and operating conditions of electrospinning. Low humidity can completely dry some type of solvent and increase the rate of its evaporation. On the contrary, high humidity will lead to the formation of thick fibers having fairly large diameters [60].

The properties of the electrospun membrane can also be modified by the post-electrospun process such as making the polymer or solvent mixtures and adding additives or crosslinking agents which can improve the mechanical properties of the fibers and their degradation. The main objective of the electrospinning process is to obtain smooth, continuous nanofibers that

do not contain beads. Thus, it is necessary to adjust the various parameters of the process and the various properties of the solution to be electrospun. Numerous studies have been carried out in order to determine the links between the parameters of the process and the morphology of the resulting fibers. Some links have been demonstrated; however, no rule has yet been clearly defined.

4. Nanofiber Imaging

The different range of diameters of silk nanofibers were obtained by varying the electrospinning parameters (solution, process and environmental parameters). Fiber diameter as well as morphology were observed using scanning electron microscopy (SEM) images obtained with the ImageJ (National Institute of Health) image analysis software. For SEM measurements, nanofibers were observed using the Quanta 200F SEM (FEI). Images were taken at a high vacuum, with an electron beam voltage of 20 kV and a chamber pressure of 80 Pa.

In order to measure the diameter of mechanically tested silk nanofibers, the nanofiber was first transferred from the window collector to the “fork” collector. Half of the nanofiber was then deposited on the SEM sample holder, which has a carbon tape and foil over it, from the fork collector. The diameter of the fibers was measured in several locations from multiple SEM images to check the uniformity of the nanofiber. The other half nanofiber remained on the “fork” sample holder for the mechanical test.

5. Nanomechanical Testing

The mechanical test of individual silk nanofiber was performed until failure with the developed testing protocol of Dr Dzenis' lab. Individual silk fibroin nanofibers were mechanically tested to failure. The protocol for sample preparation, mechanical tests until failure and evaluation of mechanical properties of individual nanofibers was developed to perform high precision tensile testing on aligned individual nanofibers. Individual nanofibers in a wide range of diameters and 4-5 cm in length (controlled by process parameters) was electrospun onto a stainless-steel plate with a rectangular window collector and picked up by a fork type wire holder (Fig. 15a).

To avoid damaging the part tested, each nanofiber was divided into two parts (Fig. 15b), one of which was then examined using the Quanta 200 FEG SEM (FEI) to determine the diameter of the nanofibers. The fiber diameter was measured in several places from several SEM images (to ensure nanofiber uniformity) and averaged using ImageJ image analysis software (National Institute of Health).

MTS's nanomechanics testing system was used for the mechanical testing of the individual nanofibers under a constant strain rate of 0.001 s^{-1} . To avoid damaging the fibers when gripping and template cutting, a section of 5 to 10 mm of the second part of the fiber was glued using epoxy glue directly to metal strips pre-placed in the test system handles (Fig. 15b-c).

It should be noted that this method prevents the placement in the axis of nanofibers. Before testing the nanofibers, the system, in addition to internal calibration, was externally calibrated. Pre-cut pieces of sheet steel of different weights were placed on the grip while the system was placed vertically, and the compression force recorded (Fig. 15d). The force recorded during calibration the experience has changed by more than two orders of magnitude. The minimum force recorded was about 33 N, which is approximately an order of magnitude greater than the minimum forces recorded during mechanical testing of nanofibers.

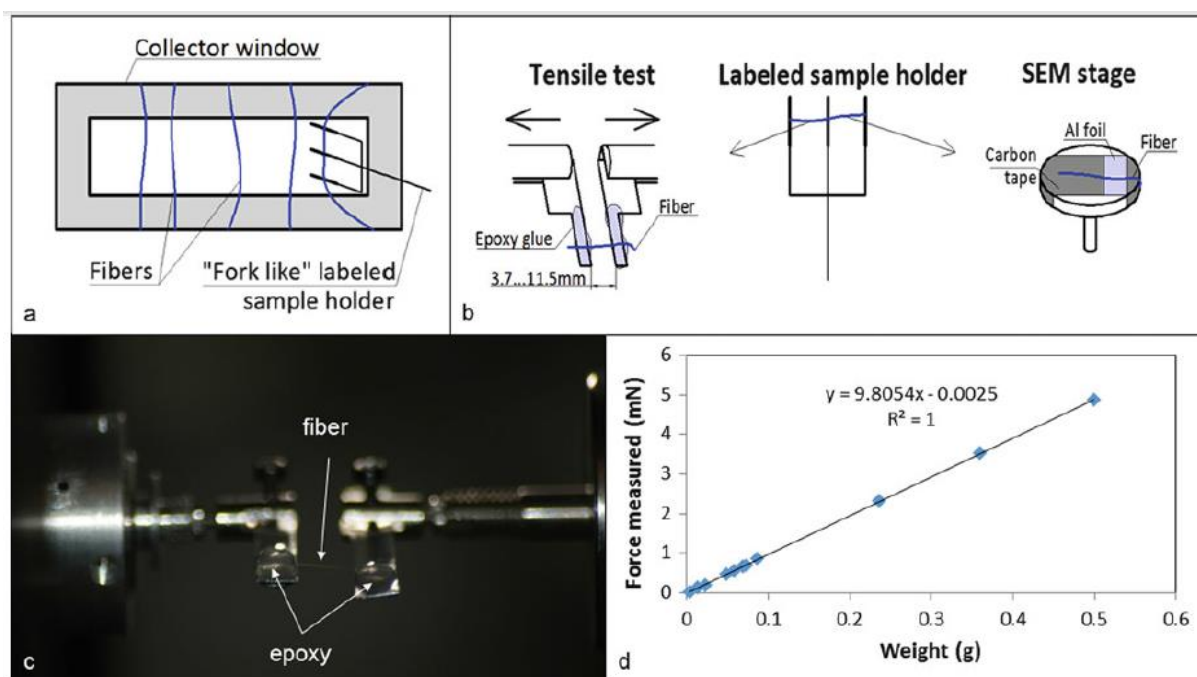


Figure 15: Sample preparation procedure and calibration of the nanomechanics testing system. (a) Schematic of the window collector and the procedure for obtaining individual NFs; (b) schematic of sample preparation for mechanical testing and diameter measurement; (c) NF mounted on the grips of the nanomechanics testing system; (d) calibration curve obtained by measuring the force exerted by pre-weighted steel foil samples [67].

6. Raman Spectroscopy

Raman spectra were recorded under vertical-vertical polarization (VV) (where the two lasers and the analyzer were vertically polarized; the fiber was also placed vertically) under ambient conditions using the LabRam Evolution Raman spectrometer (HORIBA Scientific).

The nanofibers were deposited on a microscope slide. Before depositing, the slide was covered with aluminum foil to minimize background noise. The samples were studied using the green line at 532 nm of an argon ion laser. The laser beam was focused with a 100 × objective (0.9 NA-Olympus) and produced a spot size of approximately 0.72 μm and generated an intensity of <5 mW on the sample.

The confocal hole and entry slit of the monochromator were set to 150 μm. A 600 lines / mm holographic grating was used. First order Raman spectra (1000-2000 cm⁻¹) were recorded for each sample. At least 20 individual silkworm nanofibers were used to collect separate spectra from each sample. The fluorescence background was corrected using a polynomial baseline.

The peaks of the Raman spectrum were fitted with a combined Lorentzian-Gaussian form using the LabSpec6 Raman analysis software.

7. Differential Scanning Calorimetry

The device used in this study is the DSC 204 F1 Phoenix (Fig.16), it consists of two platinum cups, one contains the sample and the other contains the reference. The temperature sensors are attached to the two cups. A control system operating through a large temperature range (from -170°C to 600°C) restores the temperature difference between the two cups by measuring the power required. This device allows users to study and measure various thermal properties of materials such as; glass-transition temperatures, melting temperatures, melting enthalpy, crystallization temperatures, crystallization enthalpy, transition enthalpies, phase transformations, phase diagrams and other thermal properties.

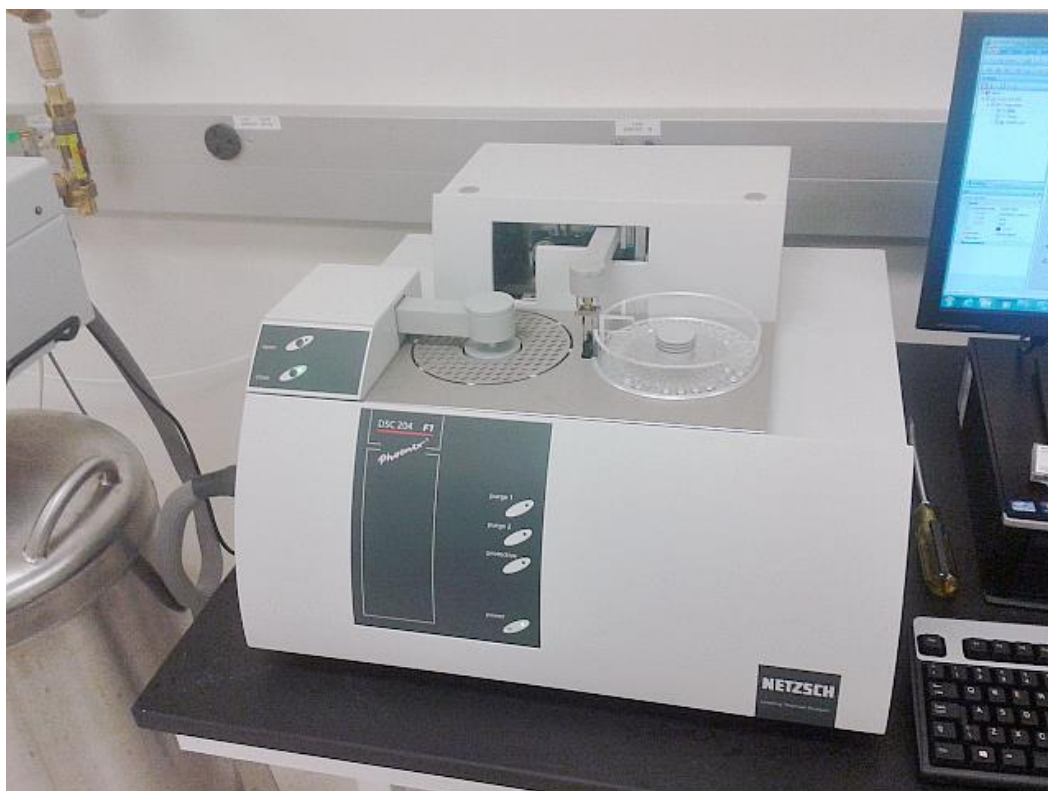


Figure 16: DSC 204 F1 Phoenix

Source : <https://ncmn.unl.edu/smcj/thermal-analysis-systems>

Chapter 4: Results & Discussion

1. Parametric Analysis of Electrospinning

The morphology and diameter of the fibers depend on a lot of different parameters (i.e., the solution viscosity, the intensity of the applied electric field, the distance between the needle and the collector, ...). The control of these parameters is fundamental regarding the acquisition of high strength nanofibers. Besides, the aim of the parametric analysis is to highlight the which electrospinning parameters are required to obtain the optimal mechanical properties of silk fibroin nanofibers.

During these tests, the reference used was a solution of 2% silk fibroin, a current of 10 kV, a flow rate of 0,25 mL/h, a distance collector-needle of 10 cm and a syringe diameter of 0,15 mm.

a. Influence of the concentration

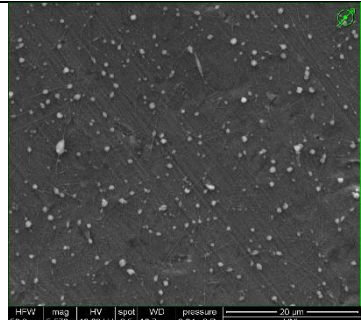
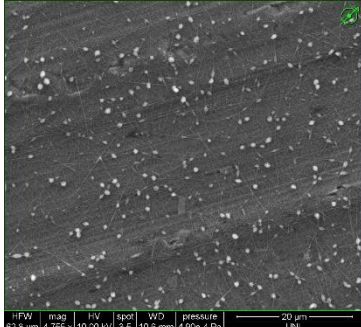
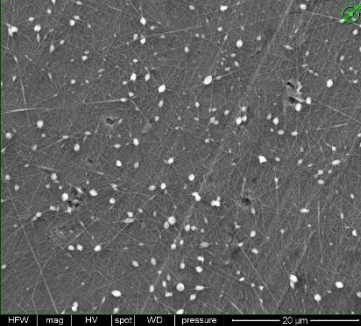
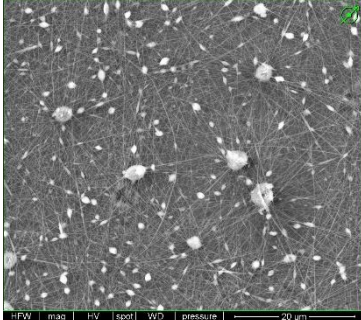
Among all the electrospinning parameters, the polymer concentration of a specific polymer system is considered to have the most influence in determining the final diameter of nanofibers. It has a direct influence on other solution parameters such as solution viscosity, surface tension, conductivity and ultimately has an impact on pattern development, elongation and solvent evaporation rate. Therefore, the fibroin concentration of the solution ultimately affects the diameter and morphology of the fibers.

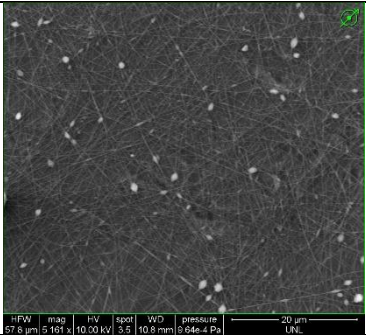
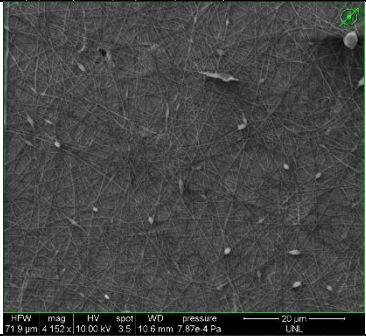
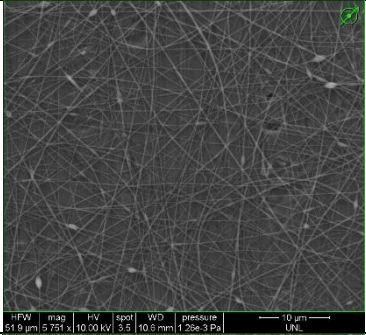
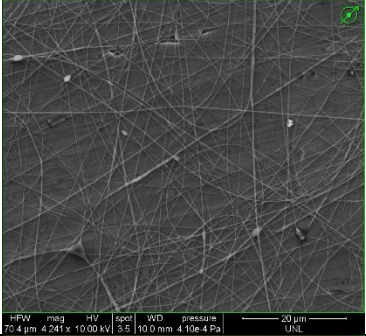
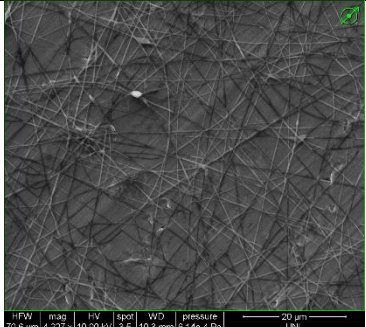
The use of different solvents also has an impact on several parameters as indicated above.

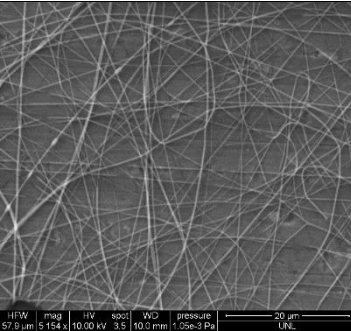
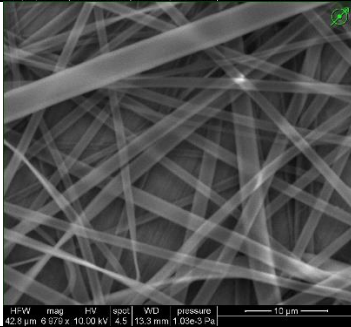
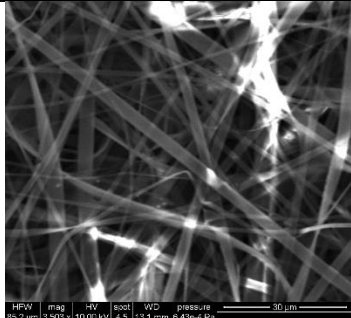
However, for this project, the effect of different solvents will not be discussed.

Here, several solutions with a broad concentration range have been studied starting at 1% silk fibroin concentration to 6% silk fibroin concentration. All of the solutions have been diluted using Hexafluoroisopropanol (HFIP). Table 3 shows the average fiber diameter as well as the microstructure of the nanofibers obtained after electrospinning for each concentration.

Table 3: Average silk nanofiber diameter and microstructure obtained after electrospinning for different concentration

silk fibroin concentration (%)	Average Diameter (nm)	Microstructure
1	31,1	
1,2	44,73	
1,4	55,01	
1,6	82,6	

1,8	95,4	
2	136,7	
2,3	155,8	
2,6	177,28	
2,8	200,53	

3	227,56	
4	1208,45	
6	2116,67	

According to these results, a lower silk fibroin concentration allows the obtention of thinner nanofibers (Fig.17). However, a phenomenon can be observed, especially for low silk fibroin concentrations: the beading of fibers. Thus, despite having a thinner diameter, the average volume of fibers will be higher than nanofibers obtained with a slightly higher solution concentration (i.e., 1,8 and 2% silk fibroin solutions). Indeed, the presence of a lot of beaded fibers induces a large volume of beads.

Therefore, the beading phenomenon was investigated to draw the threshold under which beaded fibers are prominent. It seems that the limit is reached below a solution of 1,8% of silk fibroin. Even though beaded fibers can be obtained at higher concentrations, they are not as ubiquitous as for lower concentration range (from 1% to 1,6% silk fibroin concentration).

While a solution with a high silk fibroin concentration leads to an increase in the viscosity and in the diameter of the fiber. The electrospinning process also seems to require a minimum concentration of solution for fiber formation. Since low concentration solution led to the obtention of beaded fibers. Also, if the viscosity is too high, the jet will break down into droplets and it will not be possible to form fibers, because the electrical charges will not be high enough to allow the fiber to be drawn.

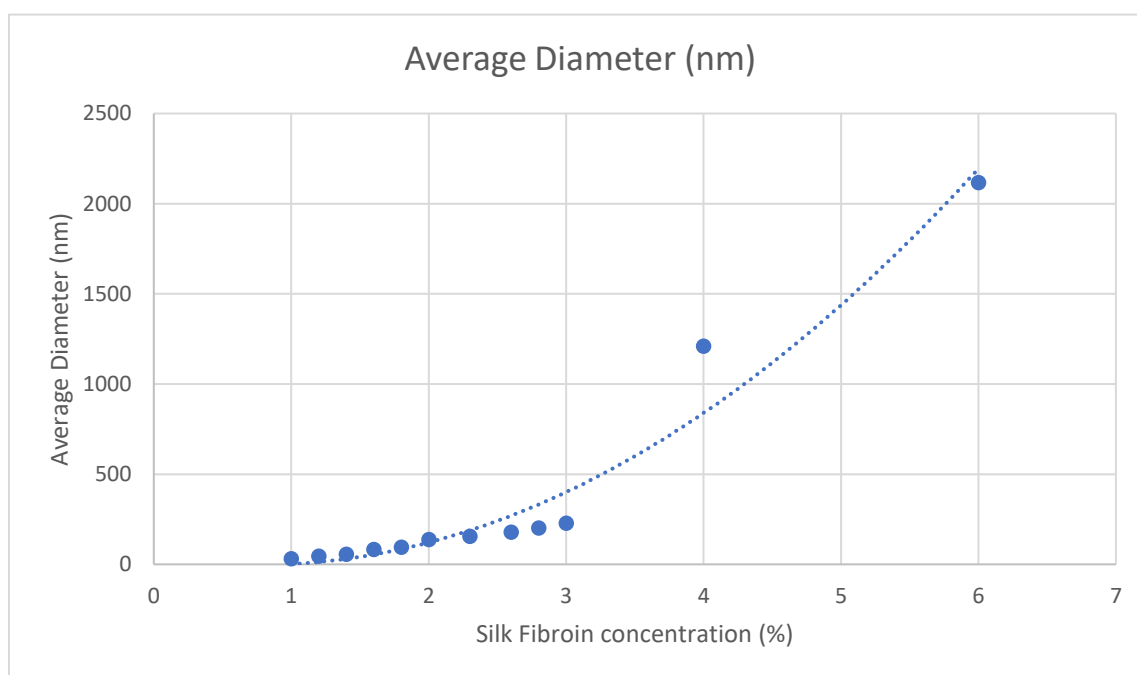


Figure 17: Average nanofiber diameter vs silk fibroin concentration

The diameter distribution of nanofibers was also investigated in order to observe diameter variability. 2% silk fibroin nanofibers were studied due to the fact that they exhibit a very small number of beaded fibers compared to lower silk fibroin concentration nanofibers. The diameter distribution of these nanofibers can be observed in Figure 18.

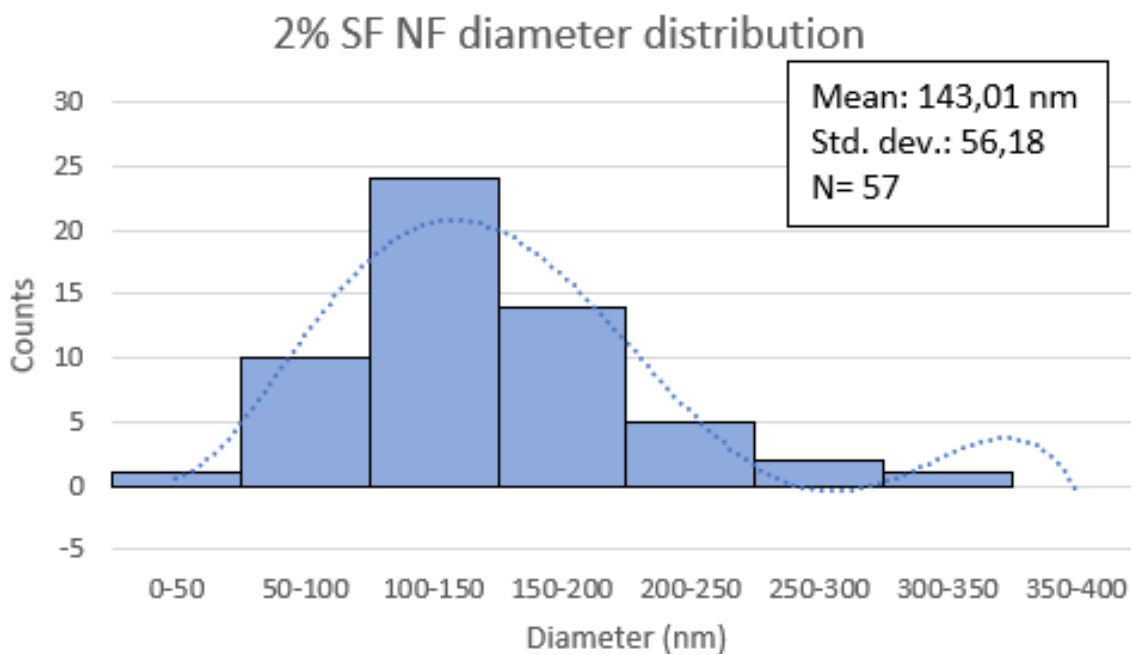


Figure 18: Diameter distribution of 2% silk fibroin nanofibers

The diameter distribution of these fibers was compared to 1% silk fibroin nanofibers diameter distribution (Fig. 19). The most noticeable difference between the two diagrams is certainly the standard deviation that is highly superior for the 1% silk fibroin nanofibers due to the presence of numerous beaded fibers. Also, the mean diameter of these fibers is also superior to the value mentioned in Table 3 for the same concentration due to the fact that the diameter of beaded fibers is taken into account.

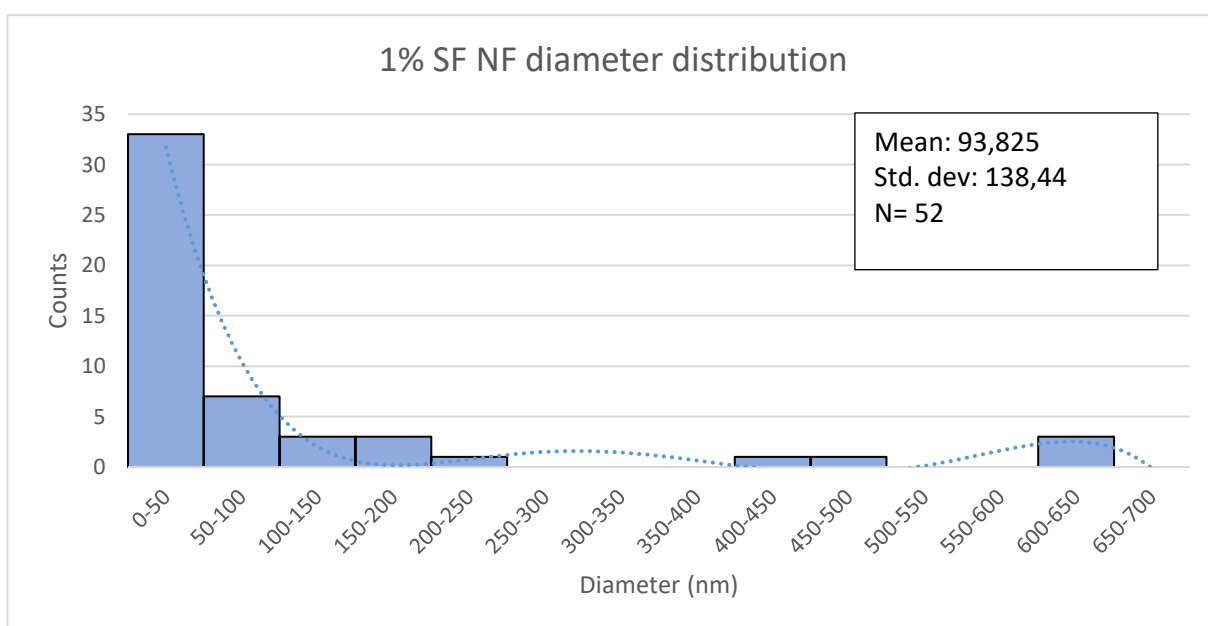


Figure 19: Diameter distribution of 1% silk fibroin nanofiber

b. Influence of the applied current

The electric field is the primary factor in the electrospinning process because it affects the amount of charge applied to the solution. It appears that the increase in tension causes an increase in the intensity of the traction on the flow of solution, which favors the formation of thinner fibers.

However, it also seems that after reaching a certain value (here 10 kV), the increase in the current during the electrospinning has the consequence that the syringe ejects more fibroin solution, which increases the diameter of the nanofibers (Table 4 & Fig. 20).

Table 4: Average diameter of nanofiber obtained for different current values

Current (kV)	Average Diameter (nm)
5	1049,44
7,5	826,3
10	698,614
12,5	977
15	1008,97

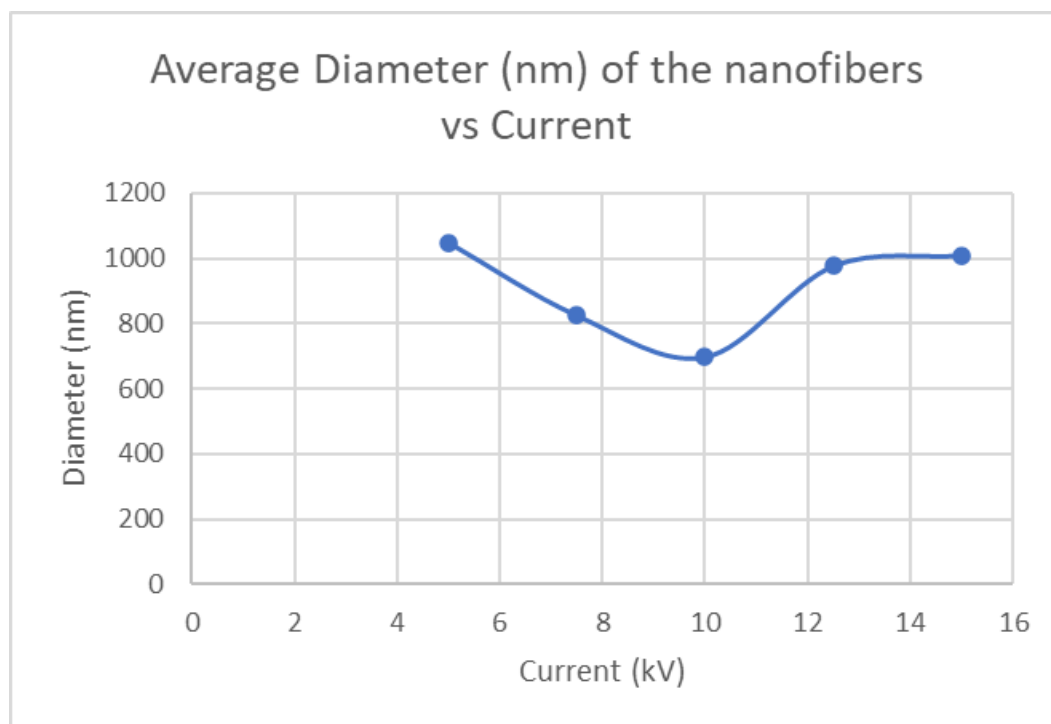


Figure 20: Average nanofiber diameter vs Applied current

However, the impact of the current applied during electrospinning on the fiber diameter is controversial. Indeed, as explained in Chapter 3. 3. b., several studies have been investigating this parameter and their results are divided. Therefore, there is no established statement about the effects of the applied current on the nanofiber diameter.

c. Influence of Flow rate

Another important parameter of the electrospinning process is the flow rate of the polymer solution inside the syringe. Generally, a low flow rate is the most recommended to have enough time for the solution to polarize. During the spinning of the silk fibroin nanofibers, a lower flow rate (0,25mL/h) enabled the obtention of thinner diameters (Table 5 & Fig. 21).

However, a balance must be kept between the rate of flow of the solution in the syringe and the rate of dispensing or ejection of the jet through the tip of the needle during electrospinning. At this optimum feed rate, the diameter distribution of the fibers is narrow and any deviation will result in the formation of fibers with large diameters. In addition, when the flow rate is very high, beaded fibers with large diameters are formed rather than smooth fibers with fine diameter (Fig. 22), this due on the one hand to the short drying period before reaching the collector and on the other hand by the weak stretching force.

Table 5: Average diameter of nanofiber obtained for different applied flow rate

Flow Rate(mL/h)	Average diameter (nm)
0,25	698,614
0,5	747,76
1	769,7
2	818,424

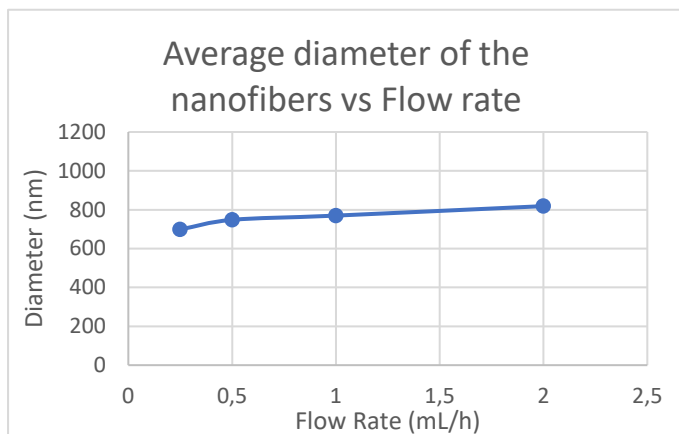


Figure 22: Average nanofiber diameter vs applied flow rate

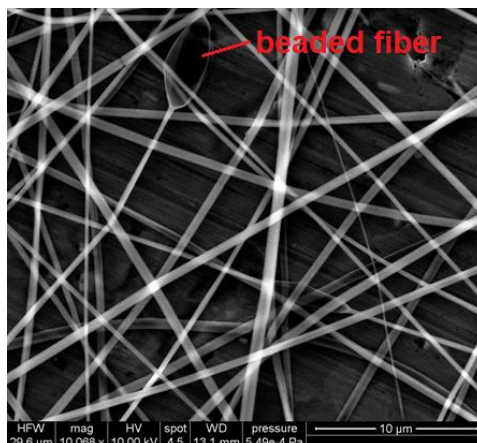


Figure 21: Microstructure of nanofibers obtained for a flow rate of 1mL/h

d. Influence of the distance needle - collector

The distance between the collector and the end of the needle can also affect the diameter and morphology of the fiber. During the electrospinning of silk fibroin, results showed that if the needle / collector distance is too short, the fiber will not have enough time to solidify before reaching the collector which will cause the fibers to increase in diameter. Conversely, if the distance is too long, circular beaded fibers can be obtained (Table 6 & Fig 23).

Table 6: Average diameter obtained for a specific distance needle - collector

Distance needle - collector (cm)	Average diameter (nm)
7	962,4
10	698,614
12	730,74
15	893,2

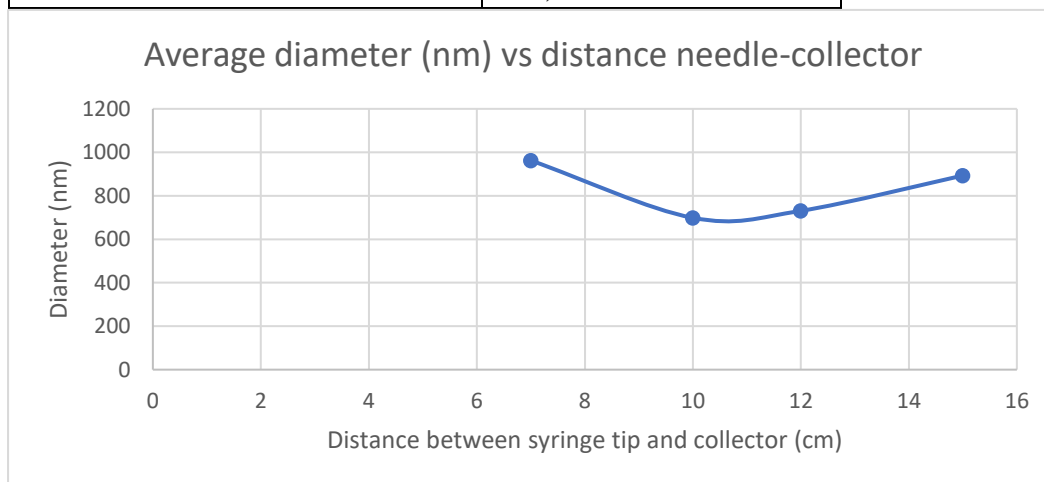


Figure 23 : Average nanofiber diameter vs distance needle - collector

e. Influence of needle diameter

The needle diameter seems to have an impact on the nanofiber diameter as well. According to the results, a thinner needle diameter enables to obtain thinner nanofibers (Fig. 24). However, the very thin diameters shown in Table 7 can be explained by the solution concentration. Indeed, even though the solution used for electrospinning had a concentration of 2%, there were still a lot of undissolved particles in the solution. Thus, the concentration of the solution was lower than 2%. Beaded fibers were obtained in the process supporting the fact that the solution concentration was not at 2%.

Table 7: Average diameter obtained for different needle diameter

Needle diameter (mm)	Average diameter (nm)
0,15	62,6375
0,22	69,325
0,41	98,314
0,64	116,35

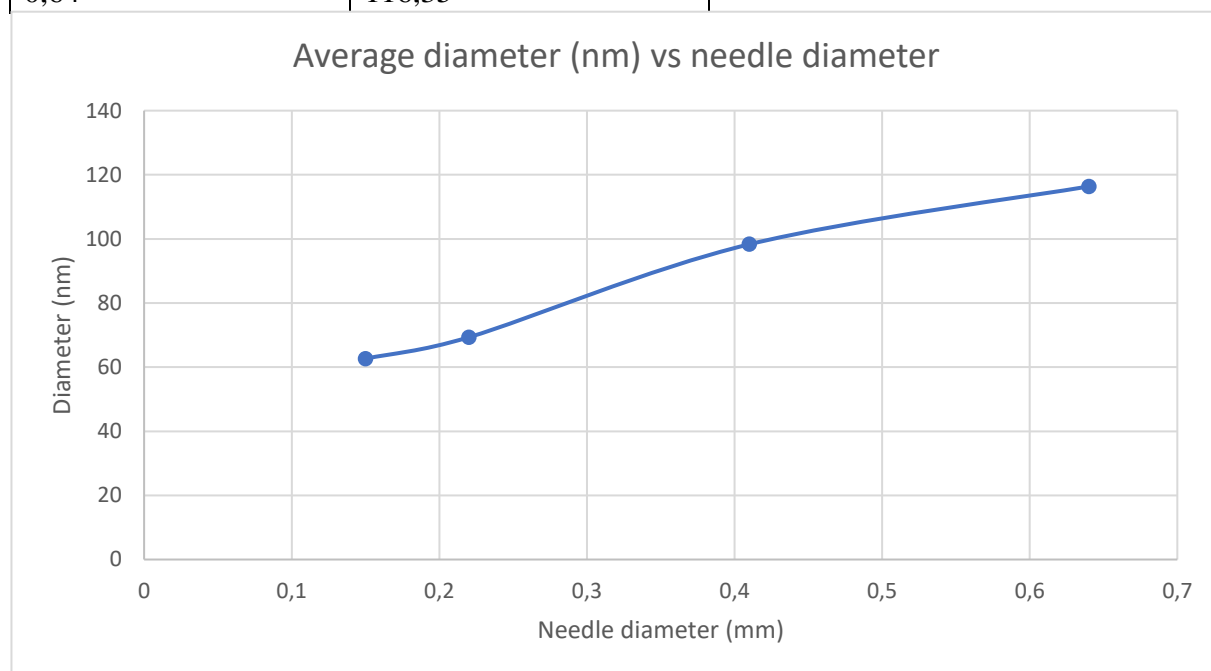


Figure 24: Average nanofiber diameter vs needle diameter

Finally, although many electrospinning parameters influence the final diameter of the silk nanofibers, only the viscosity of the solution has a considerable impact on the size of the latter. However, although a smaller diameter leads to better mechanical properties (as described in the Nanomechanical Testing paragraph), obtaining such a diameter results in the

appearance of beaded fibers. These beaded fibers are undesirable and cannot be properly exploited. In addition, their large number leads to a poor distribution of their diameter.

In addition, optimizing the diameter of the fibers (obtaining a smaller diameter and reducing the number of beaded fibers) must go through control of the various parameters mentioned above. Other parameters can also have an impact on the diameter of the fibers and its distribution, for example humidity, temperature or even the use of different solvents. It is therefore necessary to know the influence of such electrospinning parameters in order to have the best possible fiber properties.

2. Nanomechanical Testing

In order to characterize the mechanical properties of the electrospun nanofibers, nanomechanical test have been performed following the protocol established by Dr Dzenis lab. Silk fibroin nanofibers were electrospun onto a stainless-steel plate with a rectangular window collector and a single fiber was picked up for the nanomechanical test. Half of the fiber was used for the test while the other half was observed with the Scanning Electron Microscope.

Several diameters of fibers have been tested in order to acquire enough data points for the plotting of the mechanical properties of silk fibroin nanofibers in function of their diameter. Results are shown in the below Figures 25 to 28.

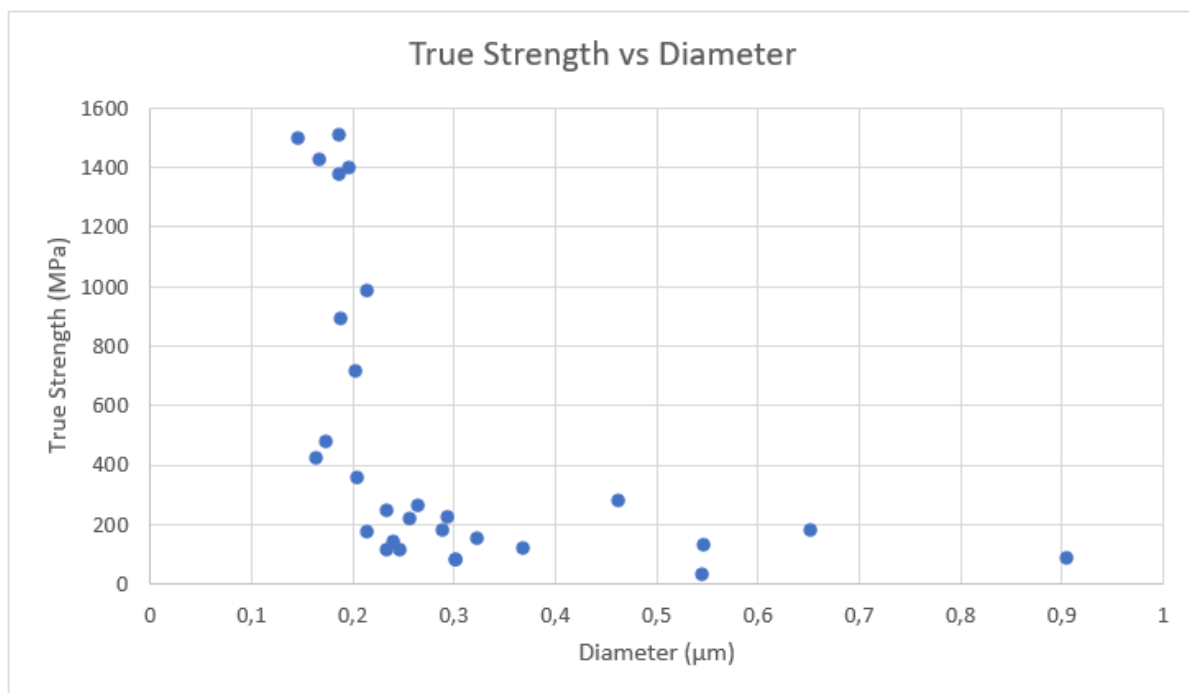


Figure 25: True strength of silk fibroin nanofibers in function of their diameter

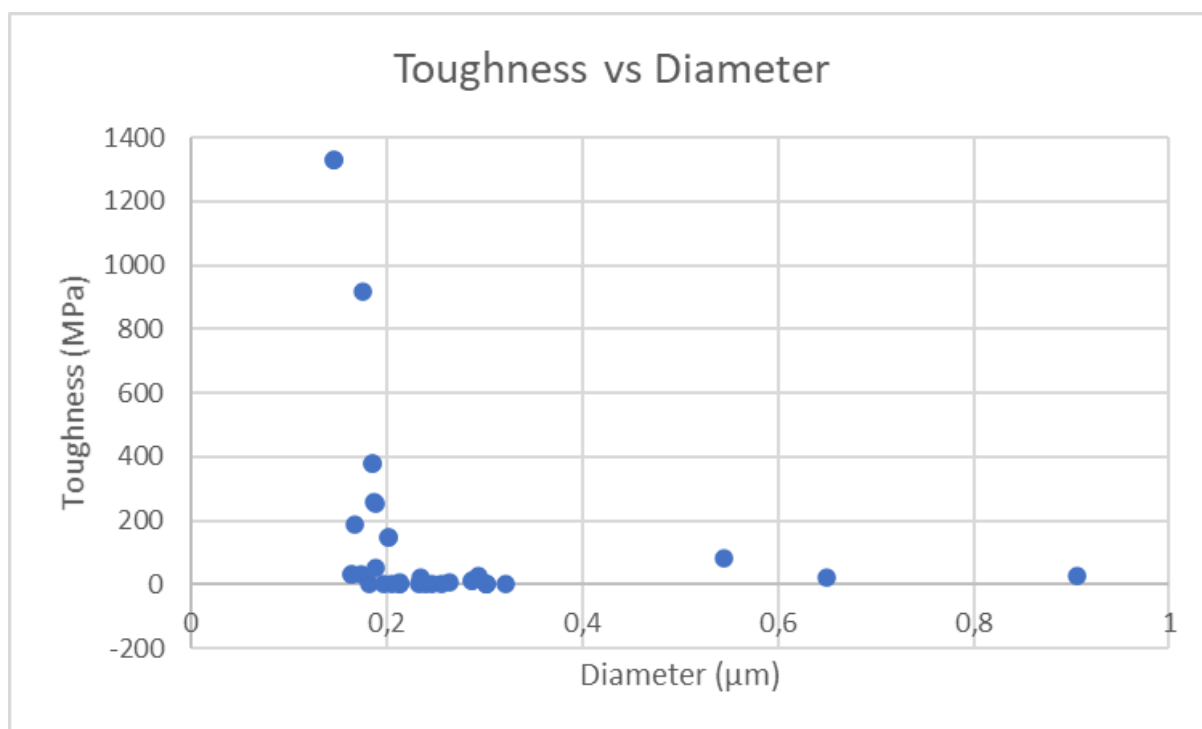


Figure 26: Toughness of silk fibroin nanofibers in function of their diameter

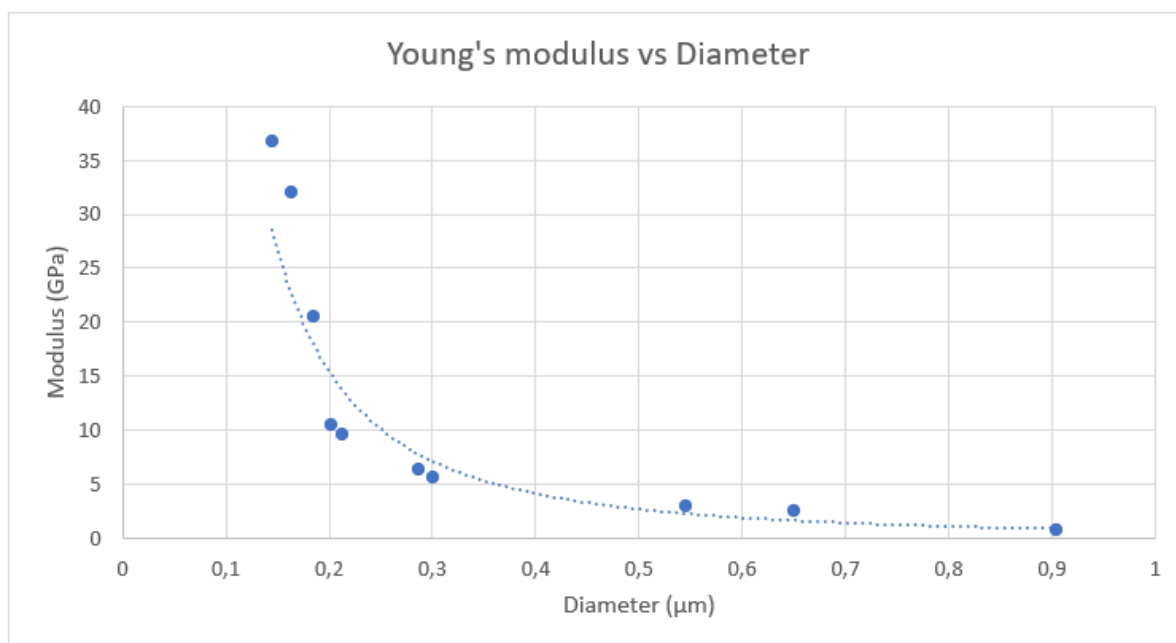


Figure 27 Young's modulus of silk fibroin nanofibers in function of their diameter

The results show a clear increase of the mechanical properties upon the reduction of the nanofiber diameter. Indeed, toughness, true strength and Young's modulus are respectively more important for a smaller fiber diameter.

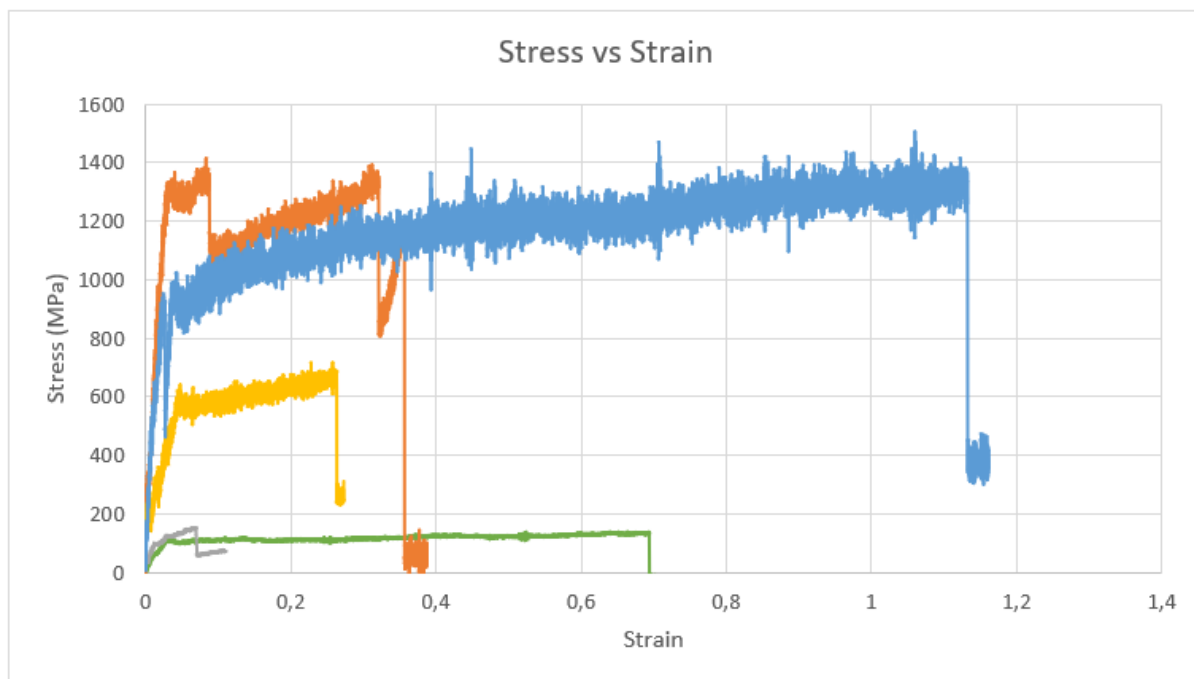


Figure 28: Stress strain curves of different diameter of nanofibers. Green: 905nm. Grey: 322nm. Yellow: 201nm. Orange: 186nm. Blue: 145nm

The stress-strain curves of these fibers mainly showed an elastic region, followed by a long plateau and a strain-hardening region until the rupture of the fiber. All the properties of these silk fibroin nanofibers were calculated from the stress-strain obtained diagrams after the observation of their diameter through SEM (calculations required the area of the sample).

Silk fibroin fibers have shown a high value of strength and strain at break which simultaneously leads to an increase in toughness. In addition, all trends analyzed in this study showed no signs of saturation, indicating a very high possibility of other performance improvements.

Moreover, a description of the mechanical properties of fibers that is more faithful to reality can be established by drawing up the true stress-strain curves of the previous nanomechanical tests. Indeed, when the fiber is stretched, the diameter is gradually reduced, thus influencing the stress undergone by the latter. So, to represent this behavior more faithfully, true stress and true strain are used and calculated using the following equations:

$$\text{True Strain} = \ln(1 + \text{Engineering Strain})$$

$$\text{True Stress} = \text{Engineering Stress} \times e^{\text{True Strain}}$$

As a result, new curves could be plotted (Fig. 29), exhibiting higher mechanical properties compared to the engineering stress-strain curves.

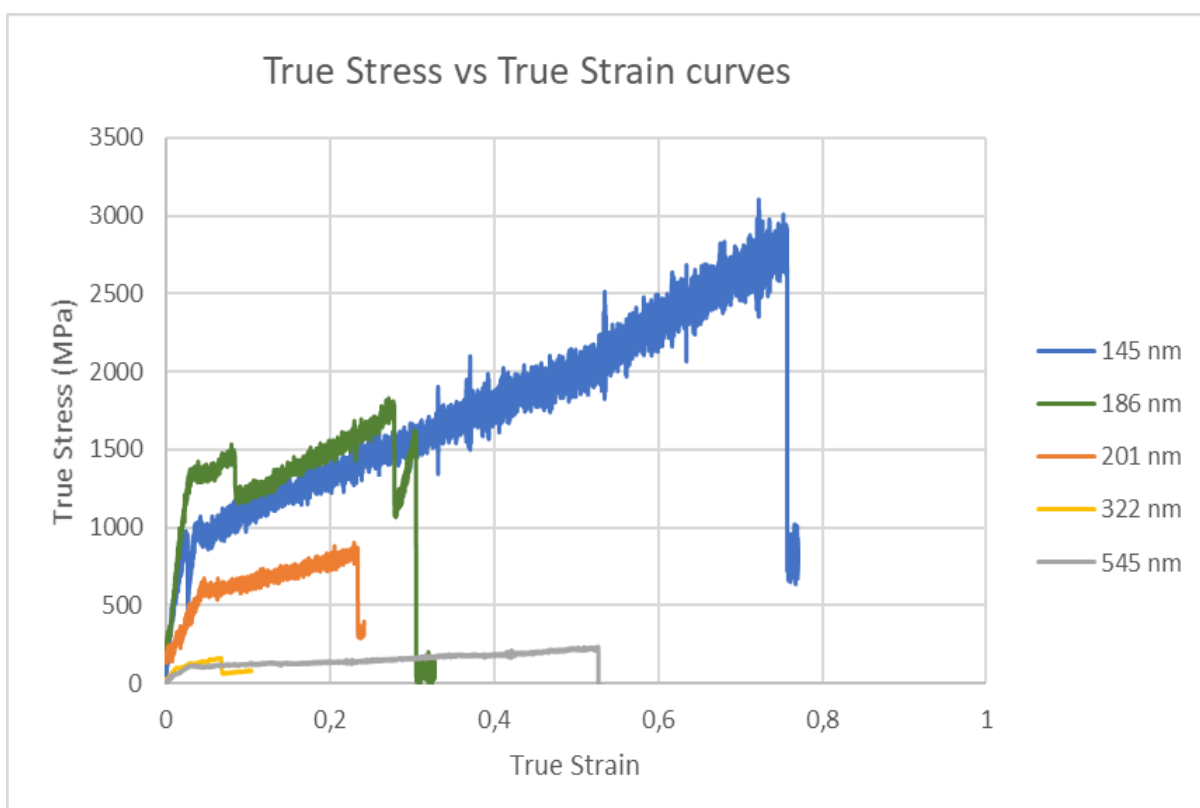


Figure 29: True stress strain curve of silk fibroin nanofibers

These curves, and especially the one describing the behavior of a 145 nm nanofiber to tensile forces can be compared to the true stress-strain of natural spider silk (Fig. 30). The results show that the 145-nanometer-diameter nanofiber can withstand twice as much strain as a spider's silk thread.

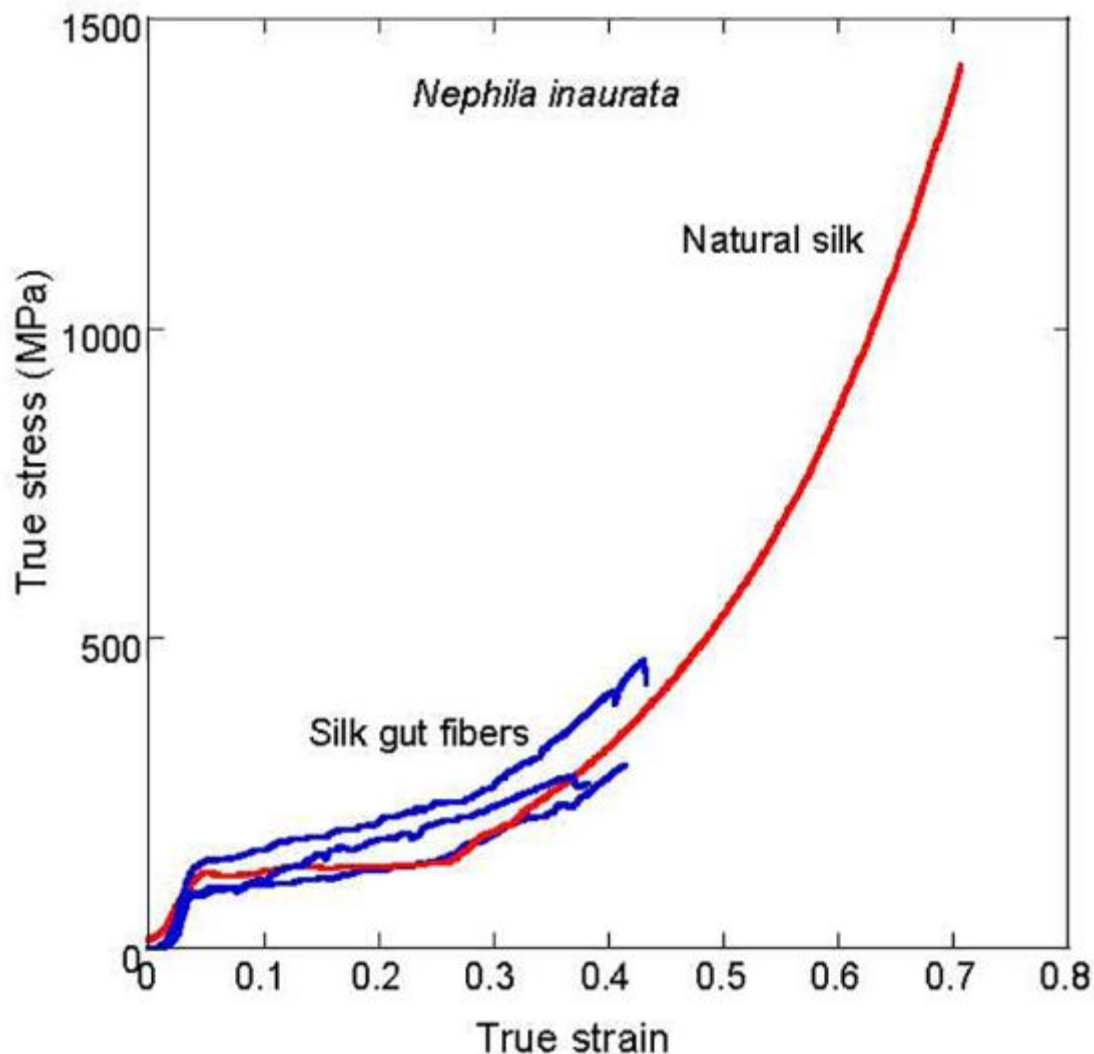


Figure 140: Comparison of the true stress-true strain curves of natural spider silk and spider silk gut fibers [68]

Furthermore, other natural single fibers have also been investigated (Fig. 31). The Figure allows to distinguish the enormous difference in mechanical property between nanofibers and these latter.

A significant gap in mechanical properties between natural fibers and silk fibroin nanofibers can be observed. The highest resistance and modulus values of measured silk nanofibers are 5-7 times higher than the typical commercial silkworm silk of *Bombyx mori* cocoons and on par with the highest reported strength and modulus of others fiber like Kevlar [69-70].

However, the stress-strain curve of the hair is not representative of reality since the slippage of the hair fiber in the epoxy has happened for every nanomechanical test. The end of its test

corresponds to the slippage of the hair rather than its rupture. Besides, literature values for hair usually reach an ultimate strength of 200 MPa [71].

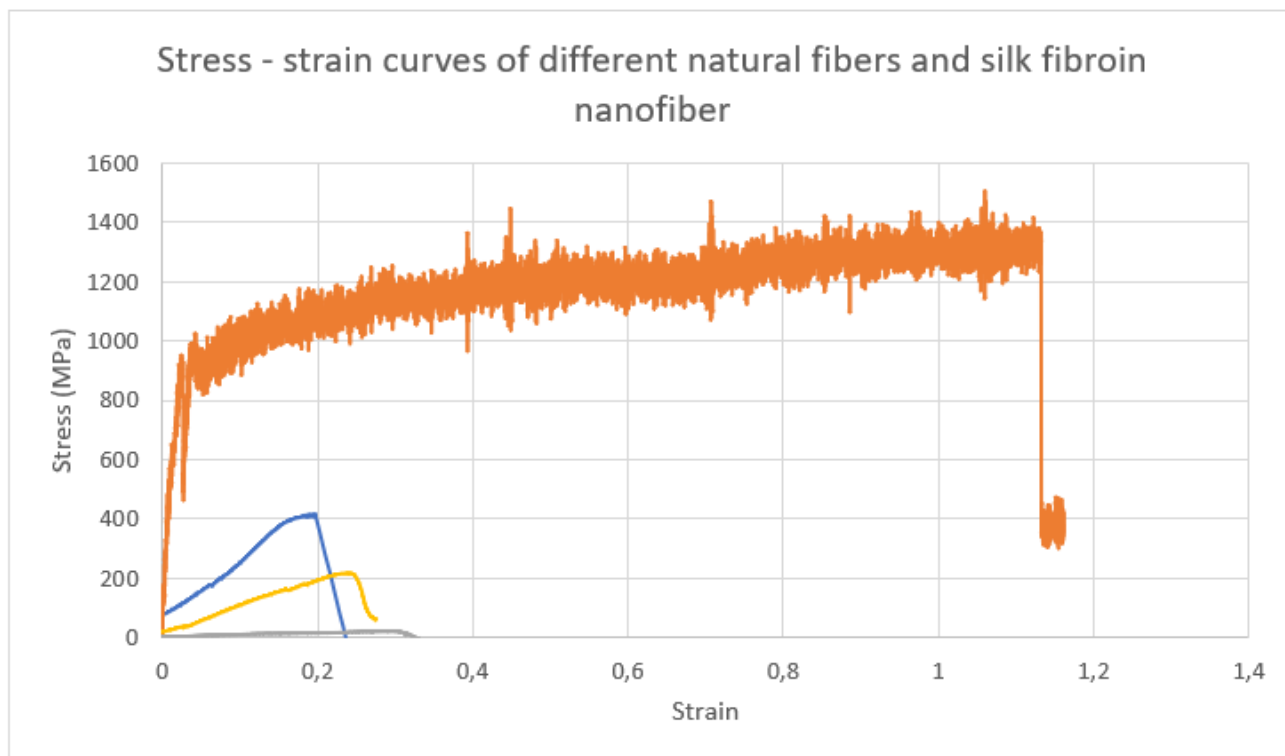


Figure 31: Stress-strain curves of natural fibers. Grey: hair (42,2 μm). Yellow: Cotton (12,87 μm). Blue: Degummed Silk (11,3 μm). Orange : silk fibroin (145 nm)

Thus, the high mechanical properties observed testify to the incredible potential of silk nanofibers which could lead to new revolutionary technical and medical applications. However, the mechanical aspect of these nanofibers is not the only parameter to be taken into account for their development. Indeed, their thermal properties also play an important role and must be carefully studied. In addition, the potential bio composite applications of these nanofibers will require control of the alignment, an essential parameter of any composite material. Measures will have to be put in place to control this alignment of the nanofibers such as for example the use of a rotating cylindrical collector during the electrospinning process (parameter which was not tested during this study).

3. Raman Spectroscopy

Raman spectroscopy is an important tool for studying the deformation of polymer fibers. It provides well-defined Raman spectra obtained from highly oriented and high modulus polymer fibers. When such fibers are deformed, the bonds in the backbone chains are strained, resulting in a decrease in the wavenumbers of the bands with Raman activity by an amount $\Delta\nu$, depending on the material, the modulus, the structure of fibers and the band considered. Figure 32 shows typical Raman spectra obtained for pure silk and silk fibroin.

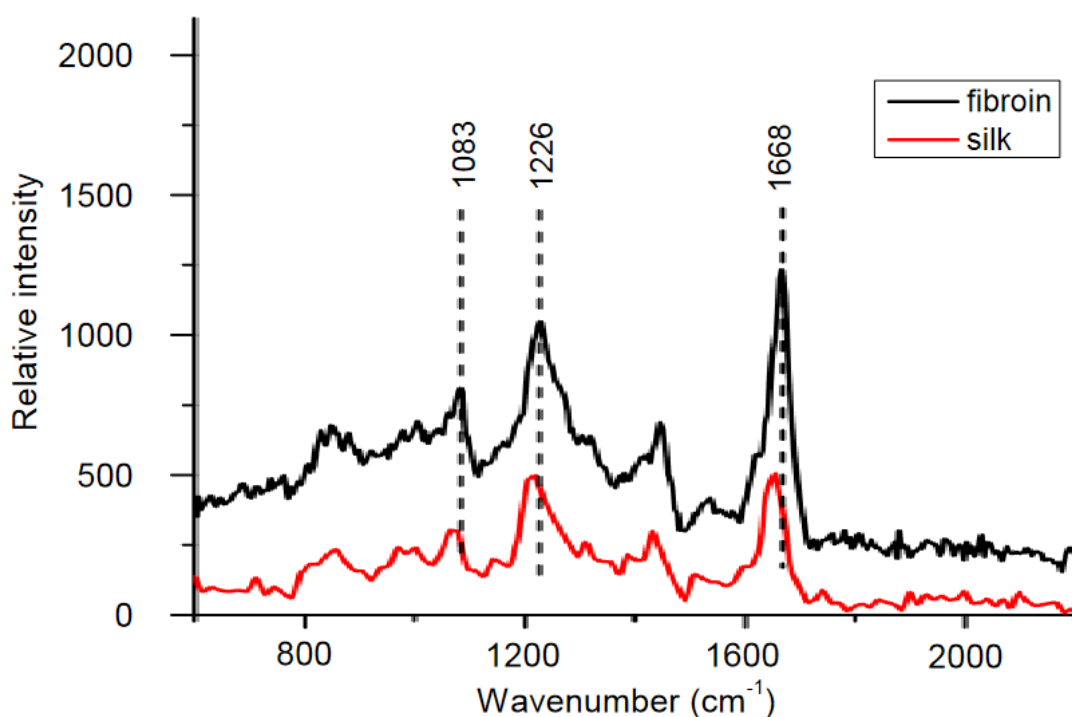


Figure 32: Raman spectra of silk (red) and fibroin (black) fibers [72]

Raman spectra of 2% silk fibroin nanofibers and degummed silk fibers of silkworm and in the range of 800-1800 cm^{-1} are shown in Figure 33. The most prominent Raman-active bands are located approximately at 1085, 1232, and 1669 cm^{-1} for degummed silk. These bands have been allocated in previous studies and are characteristic to the vibrational modes of the proteins in silk fibroin and their allocations are shown in Table 8 [73-74]. 1232 cm^{-1} and 1667 cm^{-1} bands correspond to the β -sheets in the silk fiber, i.e., the silk II conformation, and the 1085 cm^{-1} band corresponds to random-coil conformation.

For 2% silk fibroin nanofibers, the same specific bands can be observed for the same wavenumber. Therefore, it seems that no exterior phenomenon occurred such as fiber deformation during electrospinning. That phenomenon would result in a shift to bands to lower wavenumbers and similar behaviors have been observed for a number of different types of high-performance fibers [75-76].

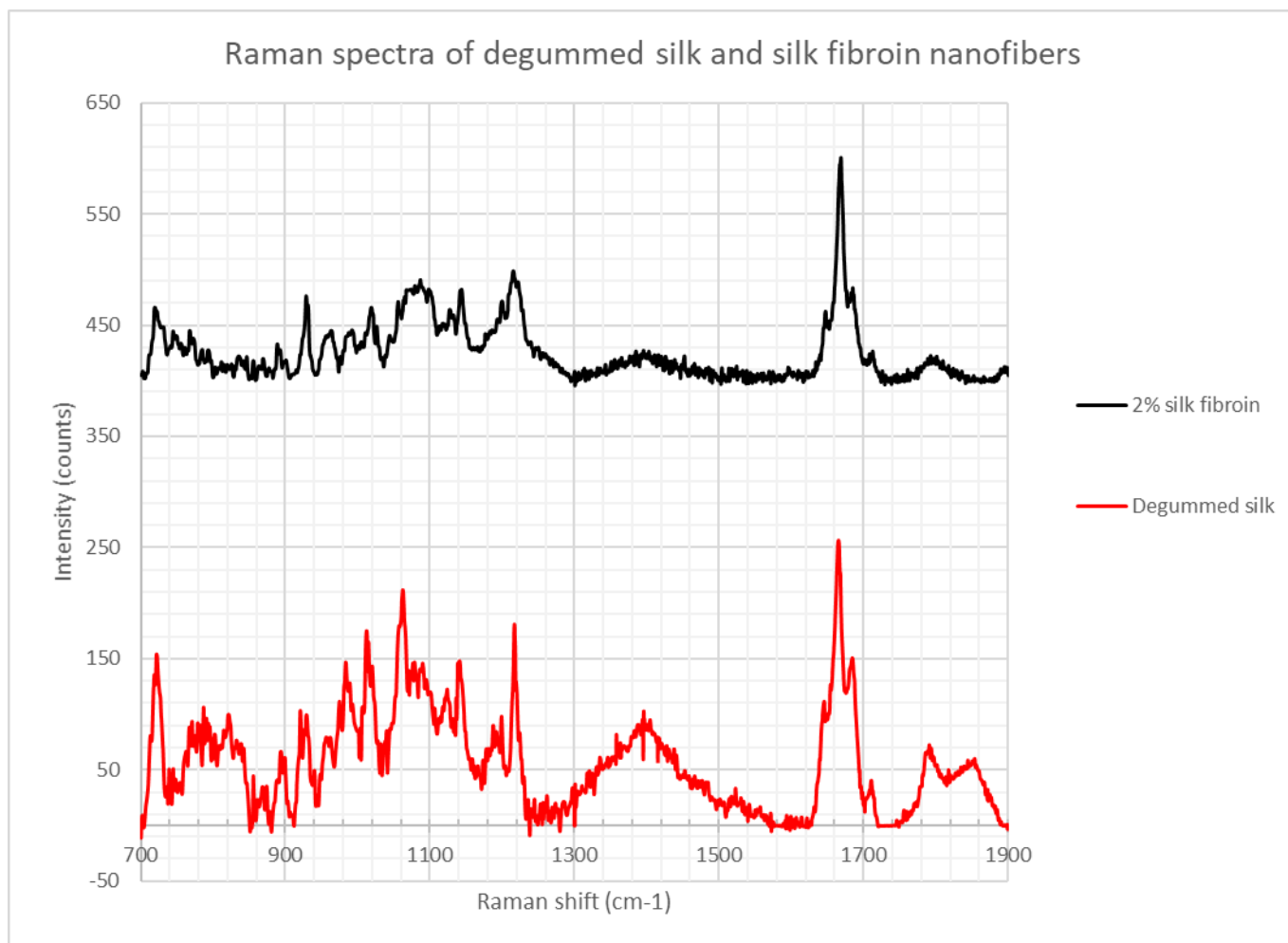


Figure 33: Raman Spectra of silk nanofibers and degummed silk

Table 8: Position and Assignment of Different Bands of Silk Proteins [77]

Band position ($\pm 1 \text{ cm}^{-1}$) ^a	Assignment
525	Ala (α -helix)
621	Phe
643	Tyr
702	C2 ^b
829	Tyr
851	Tyr
875	Pro
904	Polyalanine
921	Pro
939	α -Helix
965	Ala (β -sheet)
980	Ser
1003	Phe
1030	Phe (in-plane stretching of benzene ring)
1045	Pro
1060	Ser
1083	Ser
1102 or 1105 (1094 and 1068) ^c	Skeletal C α -C β stretching
1126	Leu
1175	Tyr
1155	C1 ^b
1207	Tyr, Phe
1260 or 1273 (1242 and 1228) ^c	Amide III
1305 (1315) ^c	Ala
1335 (1339) ^c	Ala
1369	Ala (β -sheet)
1390	C2 ^b
1399	Ala (β -sheet)
1416	Gly
1452	CH ₃ asymmetric bend, CH ₂ bending
1526	C1 ^b
1550	C2 ^b , Trp
1587	Phe
1603	Phe, Tyr-protonated form
1615	Tyr
1658 (1670) ^c	Amide I

^a Values are given for the dragline silk and may vary depending on the type of silk.

^b C1 and C2 are carotenoid and isoquinoline compounds, respectively.

^c Values in parenthesis correspond to the β -sheet conformation

Different silk fibroin concentrations have also been measured using Raman spectroscopy (Fig.34). The results show that varying the composition of silk fibroin does not affect the molecular composition and external structure of the nanofibers as the final spectra are very similar to each other. Indeed, the Raman spectra exhibit the main Raman bands of silk fibroin at the same wavenumbers, no Raman shift can be observed.

Moreover, the degree of crystallinity of the nanofibers does not seem to be affected by the change of composition of the nanofibers. The intensity and broadness of the major peaks which characterize the crystallinity of the sample is slightly fluctuating but no particular pattern seems to prevail. Indeed, the 4% silk fibroin spectrum exhibits broader and more intense peaks than other composition of silk fibroin spectra. For both higher (6% silk fibroin) and lower (2% silk fibroin) compositions, peaks are less intense. However, the crystallinity must be further investigated using Differential Scanning Calorimetry.

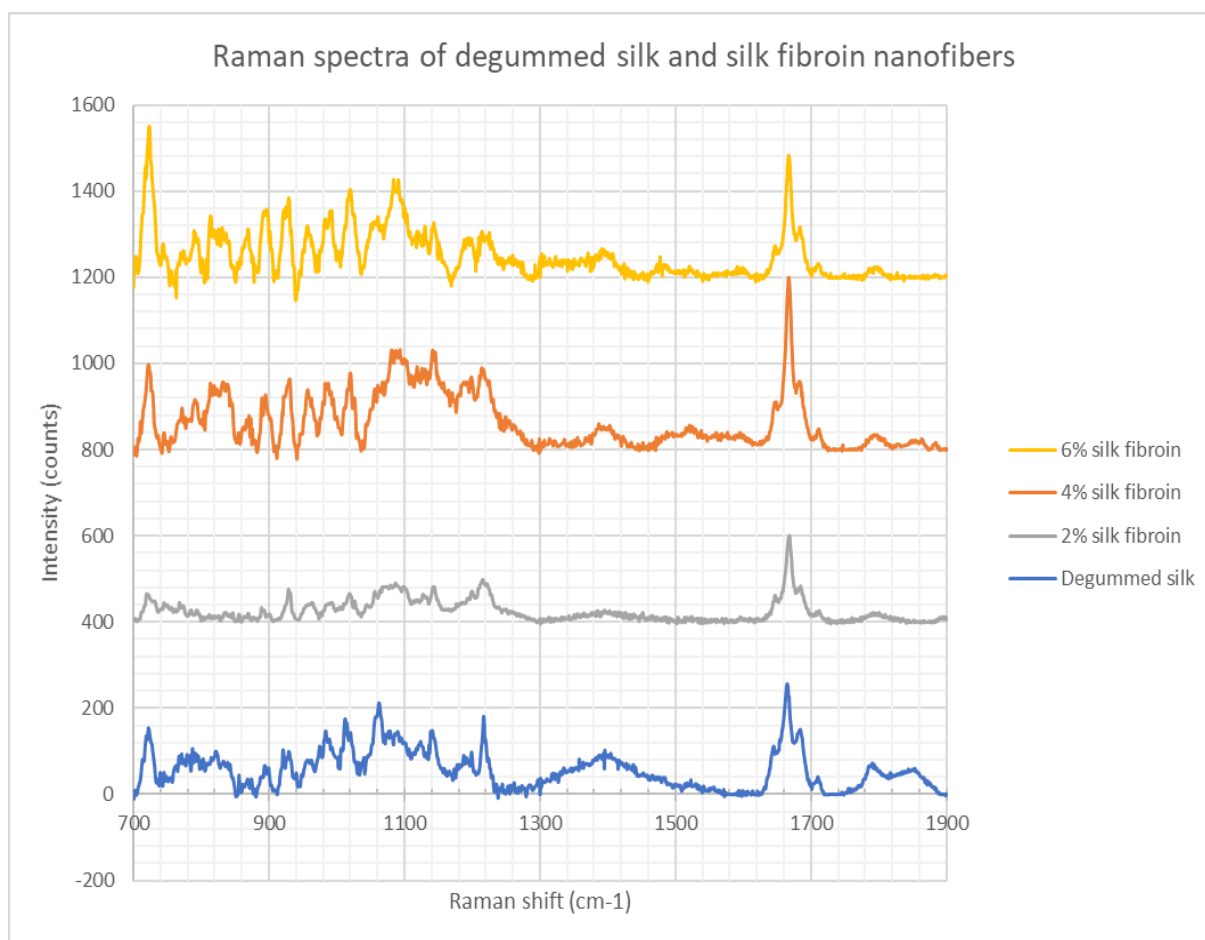


Figure 34: Raman spectra of degummed silk and of different percentage of silk fibroin nanofibers

4. Differential Scanning Calorimetry

Thermal analysis of degummed silk fibroin and silk nanofibers was presented as a differential thermal calorimetric curve (Fig. 35). The DSC curve of degummed silk fibroin exhibited a silk I T_g at 170°C with a steep slope. Also, both curves showed the presence of silk II conformation, due to the absence of peak at 230°C characterizing a mainly silk I conformation.

The two curves showed higher degradation temperatures than those reported in the literature (250 ° C for silk I and 260 ° C for silk II) [78]. In addition, a small endothermic peak can be observed at around 35 ° C, it corresponds to the peak of water evaporation. This peak is not significant here because both samples were dried before undergoing DSC analysis. However, bound water is usually found in the amorphous region of fibroin. An increase in crystallinity would cause both the evaporation temperature and the peak area to decrease.

A change in conformation by the crystallization of silk fibroin from a random coil to a β -sheet causes the existence of an exothermic curve. In the degummed silk DSC curve, an exothermic peak was observed at around 175 ° C which is attributed to conformational change of shape while an endothermic peak observed near 304 ° C is attributed to conformational change of shape in the random coils.

The decomposition peaks of the silk fibroin nanofibers (endotherms around 275 ° C) were shifted downwards relative to the degummed silk fiber, indicating the lower thermal stability of the regenerated samples. The poor thermal stability may be due to lower crystallinity as well as a decrease in molecular weight during the degumming process of regenerated fibroin materials compared to the degummed silk fiber [79].

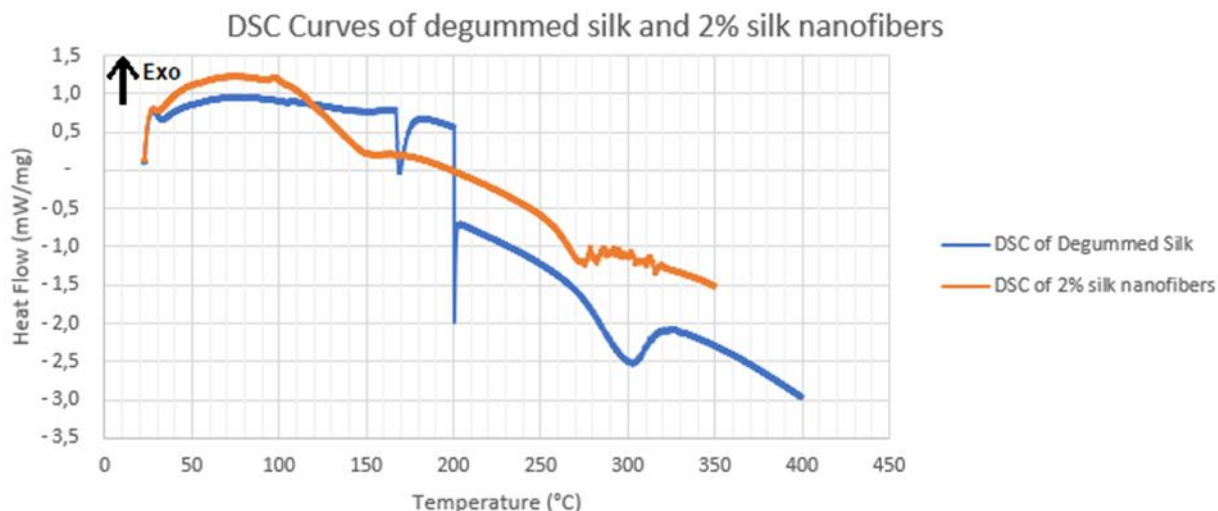


Figure 35: DSC curves of degummed silk and 2% silk fibroin nanofibers

Figure 36 illustrates other curves obtained for degummed silk and silk fibroin. [80]. One noticeable difference is that the experimental DSC curve of degummed silk exhibits a sharp drop at 200°C. Such drop was probably caused by the presence of an artifact. Artifacts are effects that are not caused by the sample under investigation. In this case, contamination of the sensors caused by residues of a sample from previous experiments could explain the shape of the artifact. The lid of the pan which bursts as a result of increasing vapor pressure of the sample could also be a probable option since such event produces an endothermic peak with a height of 0.1 mW to 100 mW depending on the quantity of gas or vapor evolved [81].

The experimental DSC curve of silk fibroin may also exhibit an artifact. Indeed, between 275°C and 320°C, an oscillating shape of the curve can be observed. It may be explained by the entry of cool air into the measuring cell due to a poorly adjusted measuring cell lid which leads to temperature fluctuations which cause a very noisy signal. Several DSC experiments should be done to obtain clearer shapes of curves.

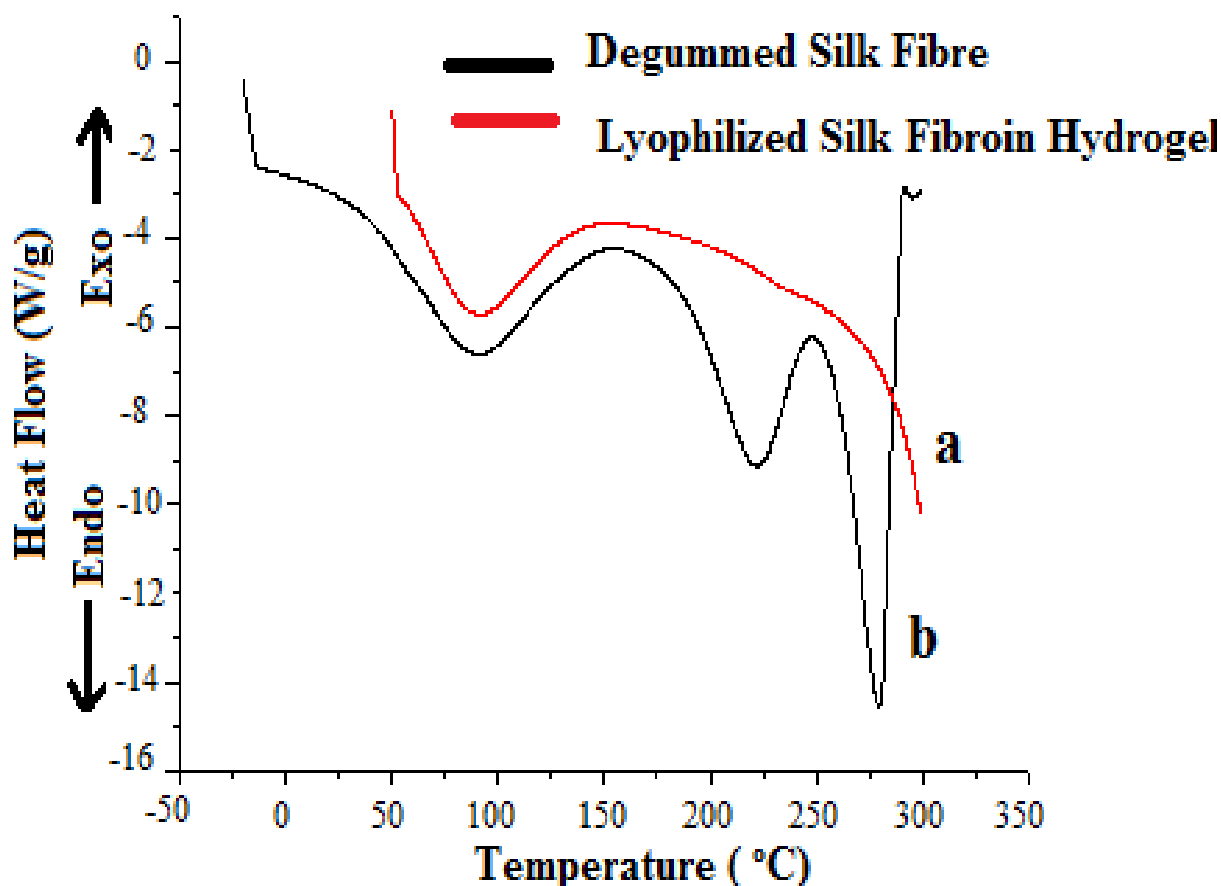


Figure 36: DSC heating curves of degummed *B. mori* silk fiber (black) and lyophilized silk fibroin hydrogel (red).

Moreover, other DSC should be performed to observe the impact of 1st and 2nd heating of the sample. This experiment could show meaningful results as the first heating scan in DSC is mostly used for removal of residual solvents, and erase the thermal history of the polymer. However, there is some exception especially for biopolymers like silk fibroins where the major transitions are obtained in the first run as gelatinization or protein denaturation occurred during the second heating.

Also, the glass-transition temperature and melting temperature can be different in first and 2nd heating as well as the crystallinity. This means that the microstructure of the silk fibroin would be different after first the heating. [82] Finally, it could provide significant information on the crystallinity of nanofibers and on the orientation of chains.

Chapter 5: Conclusion

1. Current Conclusion

Spider silk is an extremely interesting subject of study to this day, both for its incredible mechanical properties and for its development, which is still hampered by many factors. The cannibalism of spiders thus making their breeding impossible, other solutions have been considered, in particular recombinant spider silk. While researchers have succeeded in producing recombinant spider silk by inserting the silk encoder genes into other organisms, its mechanical properties are still far from those of natural spider silk. Faced with this size problem, another alternative was also considered: the production of nanofibers.

The main appeal to the nanoscale of these fibers is that it reduces the size of the defects that can lead to the material breaking, but it also reduces the probability of getting a defect on the fiber. Thus, Bombyx Mori silk was chosen for this task because their cultivation is common and inexpensive. The main objective of this research was therefore to study the properties of silk fibroin nanofibers produced by electrospinning.

A parametric study was therefore carried out on the main factors influencing the diameter of the nanofibers produced (process parameters and solution parameters). This analysis revealed the importance of the silk fibroin concentration. Indeed, a lower concentration makes it possible to obtain electrospun nanofibers of smaller size, but this also promotes the appearance of beaded fibers which are undesirable. Thus, a concentration threshold has been determined below which pearl fibers are ubiquitous. This threshold has the value 1.8 - 2% silk fibroin concentration.

The nanofibers produced were then tested using nanomechanical tests in order to obtain their mechanical properties. The results clearly show that fibers with smaller diameters have the best properties. In addition, the true stress-strain curves showed that Bombyx Mori silk

nanofibers could compete with natural spider silk in terms of mechanical properties. Indeed, these nanofibers were able to withstand a stress twice as great as a spider's silk thread. Moreover, the limits of these fibers have not yet been determined and the tendency of the curves seems to indicate that smaller nanofibers would make it possible to achieve even better properties.

2. Future work

More in-depth research must still be carried out, in particular on the composition of nanofibers and more particularly on their degree of crystallinity. For this, new differential scanning calorimetry analyzes must be carried out. Their impact on the final properties of nanofibers is also an aspect to be further explored.

In addition, a development of the electrospinning process could make it possible to better control the distribution of the diameter of nanofibers as well as their alignment for composite applications.

The phenomenon of beading of fibers is also an avenue to be investigated since their presence strongly affects the distribution of the diameter of the fibers obtained.

In addition, the influence of environmental parameters has not been studied in this report and will require further attention.

BIBLIOGRAPHY

1. Kundu SC, Kundu B, Talukdar S, Bano S, Nayak S, Kundu J, Mandal BB, Bhardwaj N, Botlagunta M, Dash BC, Acharya C, Ghosh AK. Invited review, non-mulberry silk biopolymers. *Bio-polymers*. 2012; 97:455–67.
2. Omenetto FG, Kaplan DL. New opportunities for an ancient material. *Science*. 2010; 329:528–31.
3. Hu X, Wang X, Rnjak J, Weiss AS, Kaplan DL. Biomaterials derived from silk-tropoelastin protein systems. *Biomaterials*. 2010; 31:8121–31.
4. Madsen, B., Shao, Z. Z. et Vollrath, F. (1999). « Variability in the mechanical properties of spider silks on three levels: interspecific, intraspecific and intraindividual. » *International Journal of Biological Macromolecules* 24, 301-306.
5. Vepari, C. & Kaplan, D. – Silk as a bio-material. *Progress in Polymer Science* (2009).
6. R. V. Lewis, *Chemical Reviews* (Washington, DC, United States), 2006, 106 (9), 3762-3774.
7. J. P. O'Brien; S. R. Fahnestock; Y. Termonia; K. H. Gardner, *Advanced Materials*, 1998, 10(15), 1185-1195.
8. J. G Tirrell; M. J. Fournier ; T. L. Mason ; D. A. Tirrell, *Chemical & Engineering News*, 1994, 72 (51), 40-51.
9. J. T. Prince; K. P. McGrath; C. M. Digirolamo; D. L. Kaplan, *Biochemistry*, 1995, 34 (34), 10879-10885.
10. Y. Sun; Z. Shao; P. Hu; T. Yu, *Journal of Polymer Science Part B: Polymer Physics*, 1997,35(9), 1405-1414.

11. W. A. Shear; J. M. Palmer; J. A. Coddington; P. M. Bonamo, *Science*, 1989, 246 (4929), 479-481.
12. L. R. Fox, *Annual Review of Ecology and Systematics*, 1975, 6 (1), 87-106.
13. F. Vollrath; D. P. Knight, *Nature*, 2001, 410 (6828), 541-548.
14. P. M. Cuniff; S. A. Fossey; M. A. Auerbach; J. W. Song, *Mechanical Properties of Major Ampullate Gland Silk Fibers Extracted from Nephila clavipes Spiders*. American Chemical Society: Washinton, 1994; Vol. 544, Chap, p234-251.
15. J. M. Gosline; M. W. Denny; M. E. Demont, *Nature*, 1984, 309 (5968), 551-552.
16. C. L. Craig, "Spider's web and Silk: Tracing evolution from Molecules to Genes to Phenotypes". Oxford University Press: Oxford, N.Y, 2003.
17. J. M. Gosline; M. E. DeMont; M. W. Denny, *Endeavour*, 1986, 10 (1), 37-43.
18. F. Vollrath, *Reviews in Molecular Biotechnology*, 2000, 74 (2), 67-83.
19. J. M. Gosline; P. A. Guerette; C. S. Ortlepp; K. N. Savage, *Journal of Experimental Biology*, 1999, 202 (23), 3295-3303
20. R. F. Foelix, "Biology of spiders". 2e ed.; Oxford University Press: Oxford, N.Y, 1996; p 330.
21. F. Vollrath, *Scientific American*, 1992, 266 (3), 70-76.
22. Vollrath, F., & Knight, D. P. (2001). Liquid crystalline spinning of spider silk. *Nature*, 410(6828), 541–548. doi:10.1038/35069000
23. G. H. Altman; F. Diaz; C. Jakuba; T. Calabro; R. L. Horan; J. S. Chen; H. Lu; J. Richmond; D. L. Kaplan, *Biomaterials*, 2003, 24 (3), 401-416.
24. R. L. Moy; A. Lee; A. Zalka, *American Family Physician*, 1991, 44 (6), 2123-2128.
25. N. Minoura; S. I. Aiba; Y. Gotoh; M. Tsukada; Y. Imai, *Journal of Biomedical Materials Research*, 1995, 29(10), 1215-1221.

26. J. M. Gosline; P. A. Guerette; C. S. Ortlepp; K. N. Savage, *Journal of Experimental Biology*, 1999, 202 (23), 3295-3303.
27. M. Elices ; J. Perez-Rigueiro ; G R. Plaza; G V. Guinea, *JO M Journal of the Minerals, Metals and Materials Society* 2005, 57 (2), 60-66.
28. J. P. O'Brien; S. R. Fahnestock; Y. Termonia; K. H. Gardner, *Advanced Materials*, 1998, 10(15), 1185-1195.
29. Prince, J. T.; McGrath, K. P.; Digirolamo, C. M.; Kaplan, D. L., *Construction, Cloning, and Expression of Synthetic Genes Encoding Spider Dragline Silk. Biochemistry* 1995,34, 10879.
30. Lewis, R. V.; Hinman, M.; Kothakota, S.; Fournier, M., *Expression and Purification of a Spider Silk Protein: A New Strategy for Producing Repetitive Proteins. Protein Expr. Purif* \996, 7, 400.
31. Fahnestock, S. R.; Irwin, S. L., *Synthetic Spider Dragline Silk Proteins and their Production in Escherichia coli. Appl. Microbiol. Biotechnol.* 1997, 47, 23.
32. Arcidiacono, S.; Mello, C; Kaplan, D.; Cheley, S.; Bayley, H., *Purification and Characterization of Recombinant Spider Silk Expressed in Escherichia coli. Appl. Microbiol. Biotechnol.* 1998,49, 31.
33. Voet, D.; Voet, J. G., *Biochemistry* John Wiley & Sons Inc: Toronto, 1990.
34. Scheller, J.; Gohrs, K. H.; Grosse, F.; Conrad, U., *Production of Spider Silk Proteins in Tobacco and Potato. Nul. Biotechnol.* 2001, 19, 573.
35. Scheller, J.; Henggeler, D.; Viviani, A.; Conrad, L1., *Purification of Spider Silk-Elastin from Transgenic Plants and Application for Human Chondrocyte Proliferation. Transgenic Res.* 2004, 13, 51.

36. Lazaris, A. ; Arcidiacono, S. ; Huang, Y. ; Zhou, J.-F. ; Duguay, F. ; Chrétien, N. ; Welsh, E. A.; Soares, J. W.; Karatzas, C. N., Spider Silk Fibers Spun from Soluble Recombinant Silk Produced in Mammalian Cells. *Science* 2002, 295, 472.
37. Altman, G. H.; Diaz, F.; Jakuba, C; Calabro, T.; Hran, R. L.; Chen, J.; Lu, H.; Richmond, J.; Kaplan, D. L., Silk-Based Biomaterials. *Biomaterials* 2003, 24, 401.
38. Vendrely, C; Scheibel, T., Biotechnological Production of Spider-Silk Proteins Enables New Applications. *Macromol. Biosci.* 2007, 7, 401.
39. Vollrath, F., Porter, D., & Holland, C. (2011). There are many more lessons still to be learned from spider silks. *Soft Matter*, 7(20), 9595.
40. Yuan, Qingqing & Yao, Jinrong & Chen, Xin & Huang, Lei & Shao, Zhengzhong. (2010). The preparation of high-performance silk fiber/fibroin composite. *Polymer*. 51. 4843-4849. 10.1016/j.polymer.2010.08.042.
41. Buhroo, Zafar. (2021). Latest trends in entomology and zoology studies.
42. Mondal, M & Trivedy, Kanika & Kumar, Nirmal. (2006). The silk proteins, sericin and fibroin in silkworm, *Bombyx mori* Linn. - A review. 5.
43. E. Julien, M. Coulon-Bublex, A. Garel, C. Royer, G. Chavancy, J.-C. Prudhomme, P. Couble, 2.11 - Silk Gland Development and Regulation of Silk Protein Genes, *Comprehensive Molecular Insect Science*, Elsevier, 2005, Pages 369-384, ISBN 9780444519245,
44. A. Matsumoto, A. Lindsay, B. Abedian, and D. Kaplan. "Silk fibroin solution properties related to assembly and structure". *Macromolecular Bioscience*, Vol. 8, pp. 1006–1018, 2008.
45. Yu Qi1, Hui Wang1, Kai Wei1, Ya Yang, Ru-Yue Zheng, Ick Soo Kim and Ke-Qin Zhang: A Review of Structure Construction of Silk Fibroin Biomaterials from Single Structures to Multi-Level Structures. *Int. J. Mol. Sci.* 2017, 18, 237

46. E. Iizuka. "The physico-chemical properties of silk fibers and the fiber spinning process". *Experientia*, Vol. 39 (5), pp. 449–454, 1983.
47. P.J. HERRERA-FRANCO, A. VALADEZ-GONZALEZ: 12 - Mechanical testing of natural-fiber composites, In *Woodhead Publishing Series in Composites Science and Engineering, Properties and Performance of Natural-Fibre Composites*, Woodhead Publishing, 2008, Pages 375-401,
48. Colomban, Philippe. (2012). Understanding the nano- and macromechanical behaviour, the failure and fatigue mechanisms of advanced and natural polymer fibres by Raman/IR microspectrometry*. *Advances in Natural Sciences: Nanoscience and Nanotechnology*. 4. 013001. 10.1088/2043-6262/4/1/013001.
49. Colomban, P., Jauzein, V. (2018). *Silk. Handbook of Properties of Textile and Technical Fibres*, 137–183. doi:10.1016/b978-0-08-101272-7.00005-5
50. S. Watt, I. McEwen, and C. Viney. "Stability of molecular order in silkworm silk". *Macromolecules*, Vol. 32, pp. 8671–8673, 1999.
51. N. Agarwal, D. Hoagland, and R. Farris. "Effect of moisture absorption on the thermal properties of Bombyx mori silk fibroin films". *Journal of Applied Polymer Science*, Vol. 63 (3), pp. 401–410, 1997.
52. X. Hu, D. Kaplan, and P. Cebe. "Determining beta-sheet crystallinity in fibrous proteins by thermal analysis and infrared spectroscopy". *Macromolecules*, Vol. 39, pp. 6161–6170, 2006.
53. X. Hu, D. Kaplan, and P. Cebe. "Effect of water on the thermal properties of silk fibroin". *Thermo-chimica ACTA*, Vol. 461, pp. 137–144, 2007.
54. Ribeiro M, de Moraes MA, Beppu MM, Monteiro FJ, Ferraz MP. The role of dialysis and freezing on structural conformation, thermal properties and morphology of silk fibroin hydrogels. *Biomatter*. 2014;4:e28536. doi:10.4161/biom.28536

55. Shailesh Nagarkar, Taco Nicolai, Christophe Chassenieux and Ashish Lele: Structure and gelation mechanism of silk hydrogels. *Phys. Chem. Chem. Phys.*, 2010,12, 3834-3844
56. Asmatulu, R. (2016). Highly Hydrophilic Electrospun Polyacrylonitrile/Polyvinylpyrrolidone Nanofibers Incorporated with Gentamicin as Filter Medium for Dam Water and Wastewater Treatment. *Journal of Membrane and Separation Technology*. 5. 38-56. 10.6000/1929-6037.2016.05.02.1.
57. Hadjizadeh, A., Aji, A., & Bureau, M. N. (2011). Nano/micro electro-spun polyethylene terephthalate fibrous mat preparation and characterization. *Journal of the Mechanical Behavior of Biomedical Materials*, 4, 340–351.
58. Llorens, E., Armelin, E., del Mar Pérez-Madrigal, M., del Valle, L. J., Alemán, C., & Puiggalí, J. (2013). Nanomembranes and Nanofibers from Biodegradable Conducting Polymers. *Polymers*, 5, 1115-1157.
59. Gupta, P., Elkins, C., Long, T. E., & Wilkes, G. L. (2005). Electrospinning of linear homopolymers of poly (methyl methacrylate): exploring relationships between fiber formation, viscosity, molecular weight and concentration in a good solvent. *Polymer* 46, 46, 4799-4810.
60. Thompson, C., Chase, G., Yarin, A., & Reneker, D. (2007). Effects of parameters on nanofiber diameter determined from electrospinning model. *Polymer*, 48, 6913–6922.
61. Casper, C. L., Stephens, J. S., Tassi, N. G., Chase, D. B., & Rabolt, J. F. (2004). Controlling Surface Morphology of Electrospun Polystyrene Fibers: Effect of Humidity and Molecular Weight in the Electrospinning Process. *Macromolecules*, 37, 573–578.
62. Moghe, A. K., & Gupta, B. S. (2008). Co-axial Electrospinning for Nanofiber Structures: Preparation and Applications. *Polymer Reviews*, 353-377.

63. Khenoussi, N. (2010). Contribution à l'étude et à la caractérisation de nanofibres obtenues par électroforage : Application aux domaines médical et composite. Université de Haute Alsace - Mulhouse. Mécanique, France.
64. Zhang, C., Yuan, X., Wu, L., Han, Y., & Sheng, J. (2005). Study on morphology of electrospun poly (vinyl alcohol) mats. *European Polymer Journal*, 423–432.
65. Garg, K.; Bowlin, G.L. Electrospinning jets and nanofibrous structures. *Biomicrofluidics* 2011,5, 013403
66. Mit-uppatham, C., Manit, N., & Pitt, S. (2004). Ultrafine Electrospun Polyamide-6 Fibers: Effect of Solution Conditions on Morphology and Average Fiber Diameter. *Macromol. Chem. Phys.*, 2327–2338.
67. D. Papkov, K. Maleckis, Y. Zou, M. Andalib, A. Goponenko, and Y. Dzenis (2016). Nano to Macro: Mechanical Evaluation of Macroscopically Long Individual Nanofibers. In: Prorok BC, Starman L (eds) *MEMS Nanotechnology*, Vol. 5. Springer International Publishing, Cham, pp 35–43
68. Pérez-Rigueiro, José & Ruiz, Víctor & Cenis, Jose & Elices, Manuel & Guinea, Gustavo. (2020). Lessons From Spider and Silkworm Silk Guts. *Frontiers in Materials*. 7. 46. 10.3389/fmats.2020.00046.
69. Papkov D, Zou Y, Andalib MN, et al. (2013) Simultaneously Strong and Tough Ultra fine Continuous Nano fibers. *ACSNano* 3324–3331.
70. Jutarat Sirichaisit, Victoria L. Brookes, Robert J. Young, and, Vollrath F. (2003) Analysis of Structure/Property Relationships in Silkworm (*Bombyx mori*) and Spider Dragline (*Nephila edulis*) Silks Using Raman Spectroscopy.
71. Yang Yu, Wen Yang, Bin Wang, Marc André Meyers, Structure and mechanical behavior of human hair, *Materials Science and Engineering: C*, Volume 73, 2017, Pages 152-163, ISSN 0928-4931

72. Gasymov, Oktay & Aydemirova, Arzu & Zeynal, Oktay & Aslanov, Baylar & Khalilova, Kh & Gasimov, Naghi & Mamedov, Nazim & Mamedova, Irada & Babaev, Sardar & Gasanov, Namig. (2015). IR ellipsometry of silk fibroin films on Al nanoislands. *physica status solidi (c)*. 12. 10.1002/pssc.201500005.
73. Xue, G. Laser Raman-Spectroscopy of Polymeric Materials. *Prog. Polym. Sci.*1994, 19, 317-388.
74. Edwards, H. G. M.; Farwell, D. W. Raman-Spectroscopic Studies of Silk. *J. Raman Spectrosc.* 1995,26, 901-909.
75. Young, R. J.; Lu, D.; Day, R. J.; Knoff, W. F.; Davis, H. A. Relationship between Structure and Mechanical Properties for Aramid Fibers. *J. Mater. Sci.*1992,27, 5431-5440.
76. Young, R. J.; Day, R. J.; Zakikhani, M. The Structure and Deformation-Behavior of Poly (p-Phenylene Benzobisoxazole) Fibers. *J. Mater. Sci.*1990,25, 127-136.
77. Lefèvre, T., Paquet-Mercier, F., Rioux-Dubé, J.-F., & Pézolet, M. (2011). Structure of silk by raman spectromicroscopy: From the spinning glands to the fibers. *Biopolymers*, 97(6), 322–336. doi:10.1002/bip.21712
78. Zaoming W, Codina R, Fernández-Caldas E, Lockey RF (1996) Partial characterization of the silk allergens in mulberry silk extract. *J Investig Allergol Clin Immunol*6:237–241
79. Warwicker JO (1954). The crystal structure of silk fibroin. *Acta Cryst.*, 7: 565-573.
80. Sah, Dr. Mahesh & Pramanik, Krishna. (2011). Preparation, characterization and in vitro study of biocompatible fibroin hydrogel. *AFRICAN JOURNAL OF BIOTECHNOLOGY*. 10. 7878-7892. 10.5897/AJB10.2621.
81. Interpreting DSC curves Part 1: Dynamic measurements. Information for users of METTLER TOLEDO thermal analysis systems.

82. Frydrych M, Greenhalgh A, Vollrath F. Artificial spinning of natural silk threads. *Sci Rep.* 2019 Oct 28;9(1):15428. doi: 10.1038/s41598-019-51589-9. PMID: 31659185; PMCID: PMC6817873.